Research paper

# Novel oxovanadium and dioxomolybdenum complexes of tridentate ONO-donor Schiff base ligand: Synthesis, characterization, crystal structures, Hirshfeld surface analysis, DFT computational studies and catalytic activity for the selective oxidation of benzylic alcohols

Hadi Kargar [a,*], Pooran Forootan [b], Mehdi Fallah-Mehrjardi [b], Reza Behjatmanesh-Ardakani [b], Hadi Amiri Rudbari [c], Khurram Shahzad Munawar [d,e], Muhammad Ashfaq [f], Muhammad Nawaz Tahir [f]

[a] *Department of Chemical Engineering, Faculty of Engineering, Ardakan University, P.O. Box 184, Ardakan, Iran*
[b] *Department of Chemistry, Payame Noor University, 19395-3697 Tehran, Iran*
[c] *Department of Chemistry, University of Isfahan, Isfahan 81746-73441, Iran*
[d] *Department of Chemistry, University of Sargodha, Punjab, Pakistan*
[e] *Department of Chemistry, University of Mianwali, Mianwali, Pakistan*
[f] *Department of Physics, University of Sargodha, Punjab, Pakistan*

## ARTICLE INFO

## ABSTRACT

Two new oxovanadium and dioxomolybdenum Schiff base complexes, $[V^VO(L)(OCH_3)(CH_3OH)]$ and $[Mo^{VI}O_2(L)(CH_2CH_3OH)]$, were synthesized by treating an ONO-donor type Schiff base ligand (**H₂L**) derived by condensation of 5-nitrosalicylaldehyde and nicotinic hydrazide with oxo and dioxo acetylacetonate salts of vanadium and molybdenum, $[VO(acac)_2$ and $MoO_2(acac)_2]$, respectively. The synthesized ligand and complexes were characterized by various spectroscopic techniques like FT-IR, multinuclear ($^1H$, $^{13}C$) NMR, elemental analysis and the most authentic single crystal X-ray diffraction analysis. In both complexes the geometry around the central metal ions was distorted octahedral as revealed by the data collected from diffraction studies. Theoretical calculation of the synthesized compounds were carried out by DFT as well as TD-DFT using B3LYP method by employing the Def2-TZVP basis set. The findings of theoretical data indicated that the calculated results are in accordance with the experimental findings. Moreover, the catalytic efficiencies of both complexes were investigated by oxidizing the benzylic alcohols in the presence of urea hydrogen peroxide (UHP) in acetonitrile.

## 1. Introduction

There are large numbers of metal complexes with imine-based Schiff bases which are commonly used as oxidation catalysts in various types of important organic reactions due to their commercially cheap, easy mode of preparation and outstanding chemical and thermal strength in both solid and liquid states [1-4]. Among these, oxovanadium(V) and dioxomolybdenum(VI) complexes achieved a prominent position for their utility as a catalyst in numerous oxidation reactions like, oxidation of alcohols to aldehydes and ketones, oxidation of sulfides to sulfoxides, epoxidation of olefins and hydroxylation of phenols [5-18].

The most demanding reactions in organic synthesis are the selective oxidation for the conversion of primary and secondary alcohols into their respective aldehydes and ketones [19]. This is because of the importance of these carbonyls as intermediates in the synthesis of other organic compounds which are required for the preparation of medicines, artificial flavoring, perfumes, agrochemicals and different kinds of dyes [20]. The routine procedure for the oxidation of alcohols involves the reaction of stoichiometric amounts of oxidants like chromates, permanganates, nitrates and bromates based reagents, with alcohols [21-23]. There are a lot of drawbacks associated with the use of these traditional reagents, such as poor efficiency, reduced yield and generation of large amounts of environmental pollutants in the form of heavy metals wastes [24]. These synthetic protocols not only consume the

---

greater quantity of these oxidizing agents but also associated with the production of toxic side products [25,26]. In addition to this, the oxidation reactions require harsh reaction conditions like, elevated pressure of oxygen, high temperature and the use of unavoidable toxic solvents which are not only corrosive but also very dangerous from an environmental point of view [27]. In order to overcome above mentioned issues, a lot of manipulations in reaction conditions were carried out to control the rate of reaction and selectivity, accompanying the amount and nature of by-products produced [28-30]. These transformations include changes in the concentration of reactants, pressure, temperature, alternative environmentally friendly solvents, and to design and develop novel catalysts [31-34].

Consequently, catalytic oxidation schemes based on transition metals like copper, nickel, cobalt, manganese, iron, palladium, chromium and gold [35-41], along with molecular oxygen [42,43], hydrogen peroxide [44] and *tert*-butyl hydroperoxide (TBHP) [45,46], as oxidizing agents, were investigated.

In addition to above listed transition metal ions having high catalytic potential with $H_2O_2$, the metals with high oxidation states like oxovanadium(V) and dioxomolybdenum(VI), have shown better potential for catalytic oxidation of benzyl alcohol owing to their greater attribution with peroxide to make catalytically active intermediates [47-54]. These metal peroxy intermediates can easily shift the oxygen atom to the substrate to oxidize it [55]. Keeping in mind the greater affinity of VO (V) and $MoO_2$(VI) complexes in the catalytic oxidation reactions, it can be predicted that oxidation of benzylic alcohols to aldehydes or ketones in the presence of urea hydrogen peroxide under lenient reaction conditions can carried out with the help of oxovanadium(V) and dioxomolybdenum(VI) complexes [56].

In continuation to our previous researches and work on Schiff base complexes for oxidation of organic compounds [57-60], we are hereby describing the synthesis, spectroscopic characterization, crystal structure, computational studies and catalytic potentials of two novel oxovanadium(V) and dioxomolybdenum(VI) complexes derived from nicotinic hydrazides.

## 2. Experimental

### 2.1. Materials and methods

All the chemicals employed in the current work were 99.9% pure and purchased from well renowned suppliers like Sigma-Aldrich and Merck. Elemental analysis was carried out by Heraeus CHN-O-FLASH EA 1112 instrument. $^1$H and $^{13}$C NMR spectra were measured at ambient temperature by using BRUKER AVANCE 400 MHz spectrometer by using tetramethylsilane (TMS) as an internal standard. Coupling constant ($J$) and chemical shift ($\delta$) values were reported in Hz and in ppm, respectively. Fourier transform infrared spectra of the synthesized compounds were recorded by making their KBr pellets with the help of IRPrestige-21 (Shimadzu) spectrophotometer.

### 2.2. Synthesis

#### 2.2.1. Synthesis of ONO-tridentate Schiff base ligand (H₂L)

Nicotinic hydrazide (1.37 g, 10 mmol) and 5-nitrosalicylaldehyde (1.67 g, 10 mmol) were dissolved separately in an approximately 25 mL of hot methanol. After complete dissolution both solutions were mixed dropwise with continuous stirring. The resulting mixture was refluxed for round about 3 h until the completion of reaction was ensured by ongoing monitoring with the help of TLC. On allowing the reaction mixture to attain the room temperature, the product was settled down leaving behind the impurities in the solvent. Finally, the desired product was collected by filtration, aided by suction apparatus and washed thrice with cold methanol to remove impurities if any.

**H₂L:** Yield 75%. *Anal.* Calc. for C₁₃H₁₀N₄O₄: C, 54.55; H, 3.52; N, 19.57, Found: C, 54.44; H, 3.55; N, 19.64%. FT-IR (KBr, cm$^{-1}$); 3302

($\nu_{N-H}$); 1631 ($\nu_{C=O}$); 1600 ($\nu_{C=N}$); 1552, 1338 ($\nu_{N=O}$); 1294 ($\nu_{C-O}$); 1076 ($\nu_{N-N}$). $^1$H NMR (400 MHz, DMSO-$d_6$, ppm): 7.08 [1H, (H-C2), d, $^3J$ = 9.0 Hz], 7.57 [1H, (H-C12), dd, $^3J$ = 7.6 Hz, $^3J$ = 4.9 Hz ], 8.14 [1H, (H-C3), dd, $^3J$ = 9.0 Hz, $^4J$ = 2.7 Hz], 8.28 [1H, (H-C13), d, $^3J$ = 7.6 Hz], 8.57 [1H, (H-C5), d, $^4J$ = 2.7 Hz], 8.71 [1H, s, (–CH = N)], 8.77 [1H, (H-C11), br], 9.09 [1H, (H-C10), br], 12.09 [1H, (–NH), s], 12.35 [1H, (–OH), s]. $^{13}$C NMR (100 MHz, DMSO-$d_6$, ppm): 116.68 (C2), 117.02 (C6), 119.87 (C12), 123.56 (C3), 126.62 (C5), 128.47 (C9), 135.45 (C13), 139.87 (C4), 144.63 (C7), 148.64 (C10), 152.47 (C11), 161.62 (C8), 162.50 (C1).

#### 2.2.2. Synthesis of [V$^V$O(L)(OCH₃)(CH₃OH] complex

The new [V$^V$O(L)(OCH₃)(CH₃OH)] complex, **VOL**, where L = *(E)-N'-*(5-nitro-2-hydroxybenzylidene)nicotinohydrazide, was synthesized by treating VO(acac)₂ (1 mmol, 0.265 g, acac = acetylacetonate) with **H₂L** (1 mmol, 0.286 g) in methanol (50 mL). The mixture was kept under reflux for 3 h to obtain the resultant product in the form of precipitates which were filtered off and then washed thoroughly with equal amounts of water, methanol and diethyl ether. The precipitates were dried in *vacuo* and then crystallized from CH₃OH to get green colored crystals suitable for single crystal analysis.

**[V$^V$O(L)(OCH₃)(CH₃OH)] :** Yield 61%. *Anal.* Calc. for C₁₅H₁₅N₄O₇V: C, 43.49; H, 3.65; N, 13.53, Found: C, 43.37; H, 3.59; N, 13.57%. FT-IR (KBr, cm$^{-1}$); 3410 ($\nu_{O-H}$) (coordinated methanol); 1604 ($\nu_{C=N}$); 1462 ($\nu_{C=N-N=C}$); 1546, 1336 ($\nu_{N=O}$); 1313 ($\nu_{C-O}$); 1028 ($\nu_{N-N}$); 918 ($\nu_{V=O}$); 580 ($\nu_{V-O}$); 457 ($\nu_{V-N}$). $^1$H NMR (400 MHz, DMSO-$d_6$, ppm): 3.17 [3H, (–OCH₃ Coord.), s], 3.37 [3H, (MeOH Coord.), d, $^3J$ = 6.9 Hz], 4.07 [1H, (MeOH Coord.), q, $^3J$ = 6.9 Hz], 7.11 [1H, (H-C2), d, $^3J$ = 8.8 Hz], 7.65–7.69 [2H, (H-C12, H-C3), m], 7.98 [1H, (H-C5), d, $^4J$ = 2.7 Hz], 8.42 [1H, (H-C13), dt, $^3J$ = 8.0 Hz, $^4J$ = 1.8 Hz], 8.87 [1H, (H-C11), br], 9.09 [1H, (CH = N), s], 9.25 [1H, (H-C10), br]. $^{13}$C NMR (100 MHz, DMSO-$d_6$, ppm): 64.4 (C (MeOH Coord.)), 66.3 (C (–OCH₃ Coord.)), 120.7 (C2), 121.5 (C6), 124.1 (C12), 124.9 (C9), 126.1 (C3), 133.1 (C5), 134.5 (C13), 135.7 (C4), 149.0 (C10), 152.7 (C7), 155.9 (C11), 158.2 (C1), 167.8 (C8).

#### 2.2.3. Synthesis of [Mo$^{VI}$O₂(L)(CH₃CH₂OH)] complex

For the synthesis of new [Mo$^{VI}$O₂(L)(CH₃CH₂OH)] complex, **MoO₂L**, equimolar amounts of **H₂L** (1 mmol, 0.286 g) and MoO₂(acac)₂ (1 mmol, 0.330 g) were suspended in 100 mL of methanol in a round bottom flask containing a magnetic bar for steady stirring. The mixture was kept under reflux for 3 h to obtain the product in the form of precipitates which were filtered off and then washed thoroughly with equal amounts of water, methanol and diethyl ether, separately. The precipitates were dried in *vacuo* and then crystallized from CH₃CH₂OH to get orange-colored crystals.

**[Mo$^V$O₂(L)(CH₃CH₂OH)] :** Yield 72%. *Anal.* Calc. for C₁₅H₁₄MoN₄O₇: C, 39.32; H, 3.08; N, 12.23, Found: C, 39.23; H, 3.13; N, 12.31%. FT-IR (KBr, cm$^{-1}$); 3448 ($\nu_{O-H}$) (coordinated ethanol); 1612 ($\nu_{C=N}$); 1467 ($\nu_{C=N-N=C}$); 1544, 1334 ($\nu_{N=O}$); 1263 ($\nu_{C-O}$); 1033 ($\nu_{N-N}$); 933 ($\nu_{O=Mo=O}$) *asym*; 916 ($\nu_{O=Mo=O}$) *sym*; 597 ($\nu_{Mo-O}$); 476 ($\nu_{Mo-N}$). $^1$H NMR (400 MHz, DMSO-$d_6$, ppm): 1.05 [3H, (–CH₃ EtOH Coord.), t, $^3J$ = 6.9 Hz], 3.45 [2H, (–OCH₂ EtOH Coord.), m], 4.33 [1H, (–OH EtOH Coord.), br], 7.17 [1H, (H-C2), t, $^3J$ = 9.1 Hz], 7.58 [1H, (H-C12), dd, $^3J$ = 7.5 Hz, $^3J$ = 4.7 Hz], 8.33–8.36 [2H, (H-C3, H-C13), m], 8.81 [1H (H-C11), br], 8.82 [1H, (H-C5), d, $^4J$ = 2.9 Hz], 9.18 [1H (H-C10), br], 9.19 [1H, (CH = N), s]. $^{13}$C NMR (100 MHz, DMSO-$d_6$, ppm): 19.0 (C (–CH₃ EtOH Coord.)), 56.73 (C (–OCH₂ EtOH Coord.)), 120.13 (C2), 120.20 (C6), 124.04 (C12), 125.68 (C9), 129.56 (C3), 130.51 (C5), 135.60 (C13), 140.93 (C4), 148.87 (C10), 152.69 (C11), 155.98 (C7), 163.93 (C1), 167.85 (C8).

### 2.3. X-ray crystallographic analysis, data collection and structure determination of complexes

Single crystal X-ray studies of oxovanadium and dioxomolybdenum

**Table 1**
Crystal data and refinement parameters for **VOL** and **MoO₂L** complexes.

| Empirical formula | $C_{15}H_{16}N_4O_7V$ | $C_{15}H_{15}MoN_4O_7$ |
|---|---|---|
| Formula weight | 415.25 | 458.25 |
| Temperature/K | 298(2) | 298(2) |
| Crystal system | Triclinic | Orthorhombic |
| Space group | $P\bar{1}$ | $Pna2_1$ |
| $a/\text{Å}$ | 7.5401(12) | 16.0969(8) |
| $b/\text{Å}$ | 10.8288(17) | 11.0169(7) |
| $c/\text{Å}$ | 11.5037(17) | 9.8529(6) |
| $\alpha/°$ | 98.954(12) | 90 |
| $\beta/°$ | 94.591(13) | 90 |
| $\gamma/°$ | 108.217(12) | 90 |
| Volume/$\text{Å}^3$ | 873.0(2) | 1747.29(18) |
| $Z$ | 2 | 4 |
| $\rho_{calc}$ (mg/mm³) | 1.576 | 1.742 |
| $\mu$ (mm⁻¹) | 0.616 | 0.798 |
| Crystal size (mm) | $0.36 \times 0.30 \times 0.28$ | $0.32 \times 0.30 \times 0.17$ |
| $F(000)$ | 424 | 920 |
| θ range for data collection | 2.871 to 27.999° | 2.531 to 26.987° |
| Index ranges | $-10 \leq h \leq 10$, $-14 \leq k \leq 14$, $0 \leq l \leq 15$ | $-20 \leq h \leq 18$, $-14 \leq k \leq 14$, $-12 \leq l \leq 12$ |
| $(\sin \theta/\lambda)_{max} (\text{Å}^{-1})$ | 0.661 | 0.638 |
| No. of measured, independent and observed $[I > 2\sigma(I)]$ reflections | 4181, 4181, 2363 | 20070, 3811, 2856 |
| Data/restraints/parameters | 4181/0/249 | 3811/40/269 |
| $R$(int) | 0.094 | 0.035 |
| $R[F^2 > 2\sigma(F^2)]$, $wR(F^2)$, $S$ | 0.042, 0.110, 0.79 | 0.029, 0.068, 0.88 |
| H-atom treatment | H atoms treated by a mixture of independent and constrained refinements | H atoms treated by a mixture of independent and constrained refinements |
| $\Delta\rho_{max}$, $\Delta\rho_{min}$(e $\text{Å}^{-3}$) | 0.44, −0.54 | 0.34, −0.43 |

complexes were carried out on a STOE IPDS-II diffractometer by using Mo-Kα radiations monochromated by graphite. The data was collected at 298(2) K in a series of ω-scans in 1° oscillations and integrated using the Stöe X-AREA [61] software package. A numerical absorption correction was applied using the X-RED [62] and X-SHAPE [63] software for Mo complex. For V complex, absorption corrections based on multi-scan use were applied [64]. The data was corrected for Lorentz and Polarizing effects. The structures were solved by direct methods using SIR2004 [65]. The non-hydrogen atoms were refined anisotropically by the full-matrix least-squares method on $F^2$ using SHELXL [66]. The collected crystallographic data of the complexes are listed in Table 1.

### 2.4. Computational details

Theoretical calculations involving geometry optimization in the gas and solution phases, vibrational frequencies and NMR chemical shifts of ligand and its complexes were performed with the Gaussian 09 package [67] at B3LYP level of theory [68]. The solution phase was modeled by using IEFPCM by considering the solvent [69]. The standard Def2-TZVP [70] was used for all atoms in ligand and complexes. Geometry optimizations were tested by frequency analysis to ensure that they were at the minima of potential energy surface (PES). The results showed that there is no imaginary frequency. The ¹H and ¹³C NMR magnetic isotropic shielding tensors were calculated by the standard Gauge-Independent Atomic Orbital (GIAO) approach in the solution phase [71]. Chemical shift values of compounds were calculated by using B3LYP/Def2-TZVP level and IEFPCM model as implicit model of solvent and compared with experimental data in DMSO-$d_6$. The same solvent was used for all IEFPCM calculations for ligand, V and Mo complexes and TMS. Chemical shifts were calculated by subtracting the appropriate

isotropic part of the shielding tensor from that of TMS δi = σ_TMS - σi. The isotropic magnetic shielding tensors for TMS calculated in the solution phase at the B3LYP/Def2-TZVP level of theory were equal to 31.92 and 184.52 ppm for the ¹H nuclei and the ¹³C nuclei, respectively. The Chemissian program was used for drawing contour plots of highest occupied molecular orbital (HOMO) and lowest unoccupied molecular orbital (LUMO) [72].

### 2.5. General procedure for oxidation of benzylic alcohols to benzaldehydes catalyzed by VOL and MoO₂L Schiff base complexes

In a 25 mL round bottom flask equipped with a magnetic stirring bar, to a solution of benzylic alcohol (1 mmol) and catalyst (0.006 mmol) in 10 mL CH₃CN, urea hydrogen peroxide (2 mmol) was added and the reaction mixture was stirred under reflux conditions for specified interval of time. The proceedings of the reaction was monitored by TLC (eluent, *n*-hexane: ethyl acetate, 7:3). After completion, the reaction mixture was filtered and the solvent was then evaporated to get the pure targeted product by column chromatography employing silica gel as a stationary phase. All products were identified by comparing their physicochemical and spectroscopic (FT-IR and NMR) characteristics with those of authentic samples.

## 3. Results and discussion

### 3.1. Syntheses

A tridentate Schiff base ligand (**H₂L**) was prepared by treating nicotinic hydrazide with 5-nitrosalicylaldehyde in a methanolic environment. Reaction of VO(acac)₂ and MoO₂(acac)₂ with **H₂L** in methanol under reflux condition produces the required metal complexes (Scheme 1). After successful synthesis and characterization, the catalytic effectiveness of the complexes were also checked by oxidising various benzylic alcohols using UHP as a source of oxygen (Scheme 2).

### 3.2. Crystal structure determination

In **VOL** (Fig. 1, Table 1), the central V-atom is *hexa*-coordinated through phenolic and enolic O-atom of the nicotinohydrazone, oxo O-atom, O-atoms of methoxy groups and imine *N*-atom. The geometry around the coordination sphere of V-atom is slightly distorted octahedral in which equatorial sites are occupied by (N1/O1/O2/O5) atoms whereas apical sites are occupied by (O3/O4) atoms. Central V-atom is deviated by 0.3057 (1) Å from the mean plane defined by equatorial atoms whereas O-atom of oxo group (O3) and O-atom of methoxy group (O5) are deviated by 1.8913 (3) and −2.0206 (3) Å, respectively from mean plane defined by equatorial atoms. The hydrazone ligand coordinates to the vanadium metal in the dianionic form as evident from N1–C7 and O1–C1 bond lengths of 1.285(3) and 1.327(3) Å, respectively. These abnormal bond values indicate the presence of the enolate form of the amide groups. The V–O, V–N, and V = O bond lengths are within normal ranges and are comparable to those observed in similar oxovanadium(V) complexes [73–75]. Nitrophenyl ring A (C1-C6/N4/O6/O7) and pyridine ring B (C9-C13/N3) are found to be planar with respective r.m.s (root mean square) deviation of 0.0080 and 0.0068 Å with dihedral angle of 5.45 (2)° between ring A and B. This dihedral angle indicates that ring A and B are almost parallel to each other. The molecules are connected with each other in the form of dimers through O—H…N bonding to form R²₂(16) loop (Fig. 2). The dimers are interlinked through C12-H12-O1 bonding as given in Table 3. The molecules are further interlinked through more C—H…O bonding named as C10-*H*10…O6 and C14-H14A…O7 bonding to form R²₂(12) loop. In addition to H-bonding, a weak interaction of the type N—O…π is found between molecules related by inversion symmetry in crystal packing. This interaction assists in further strengthening of crystal packing as
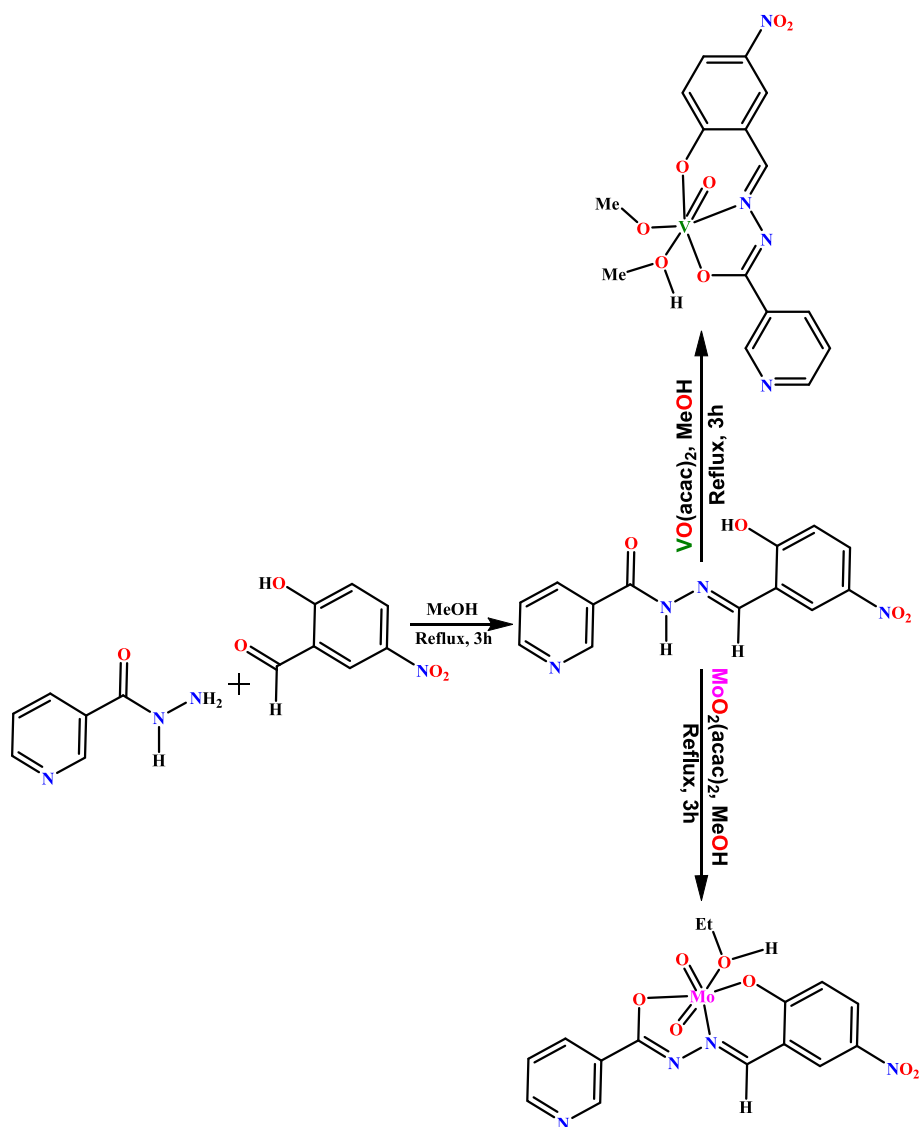
**Scheme 1.** Synthesis of ligand (**H₂L**) and its respective **VOL** and **MoO₂L** complexes.
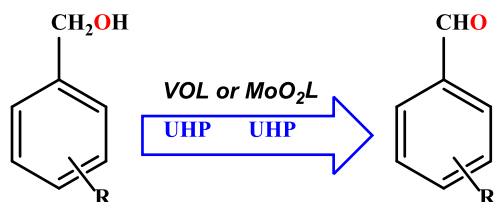


**Scheme 2.** Catalytic oxidation of benzylic alcohols in the presence of UHP by **VOL** and **MoO₂L** complexes.

displayed in Fig. 3 and specified in Table 2.

In **MoO₂L** (Fig. 4, Table 1) the coordination geometry around the molybdenum center can be described as distorted octahedral in which two *cis* positions being occupied by the two oxo groups, as bond angle O3-Mo-O4 is 105.5(2)° slightly deviates from 90°, a tridentate (ONO) dianionic hydrazone Schiff base ligand and one coordinated ethanol molecule. Hence a mononuclear dioxomolybdenum complex is formed. The distance between the molybdenum atom and the oxygen atom of the ethanol molecule, Mo1-O5 of 2.290(4) Å, represents the largest bond length within the distorted octahedron. The elongated Mo1–O5 bond length *trans* to oxo O3 group indicates weak coordination of ethanol at

the axial position which is due to the strong π-donor character of the oxo opposite to coordinated ethanol, as commonly observed in similar complexes [76]. The distortion of the octahedral coordination of the structure can also be substantiated from the bond angles related to the Mo atom. The Mo–O and Mo–N bond lengths in the complex are comparable to those observed in other oxomolybdenum complexes with hydrazone ligands [76-78]. In accordance with the previously reported studies, the bond lengths of the N1–N2 [1.1.385(6) Å] and iminic N1–C7 [1.280(6) Å] groups were increased upon coordination to molybdenum center. The two Mo = O bond distances and the subtended O(3) = Mo(1) = O(4) are comparable to the previously reported molybdenum complexes in literature [76-78]. Nitrophenyl ring A (C1-C6/N4/O6/O7) and pyridine ring B (C9-C13/N3) are found to be planar with respective r.m.s (root mean square) deviation of 0.0746 and 0.0092 Å with dihedral angle of 11.9 (2)° between ring A and B. The molecules are connected with each through O—H⋯N bonding to form a C8 chain that extends along the b crystallographic axis, where OH is from ethanol and acceptor *N*-atom is from a pyridine ring as displayed in Fig. 5 and specified in Table 2. These C8 chains are interlinked with each other through C—H⋯ O bonding in which the O-atom of one of the oxo groups acts as acceptor. Due to C—H⋯O bonding, a C7 chain is formed that extends along the b crystallographic axis.

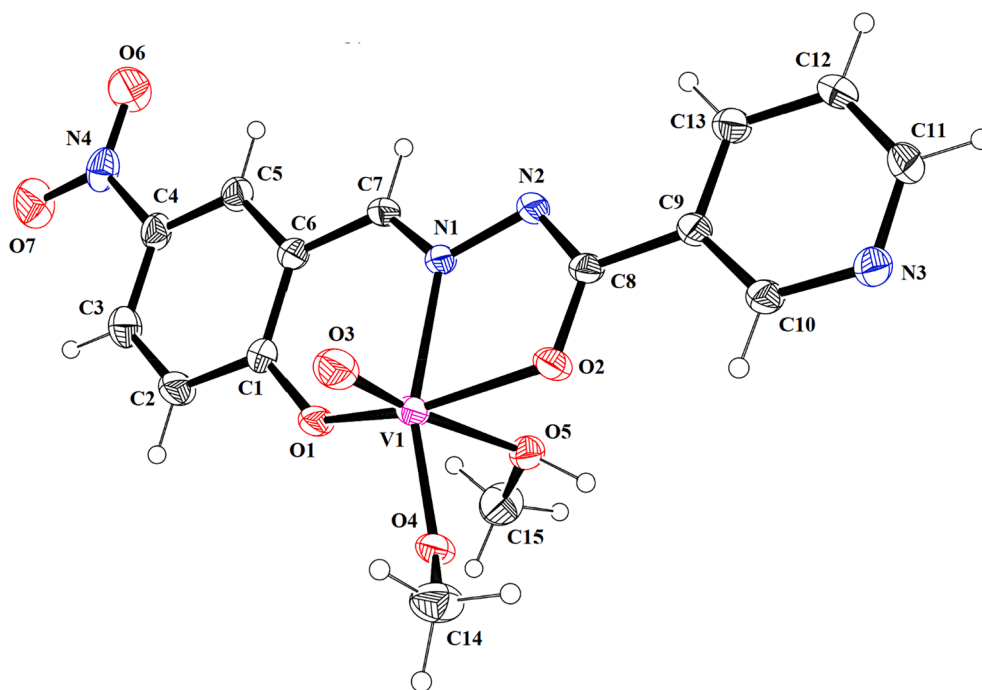Crystal Explorer version 17.5 is employed in order to perform

**Fig. 1.** ORTEP diagram of **VOL** drawn at probability level of 30%. H-atoms are shown by small circles of arbitrary radii.
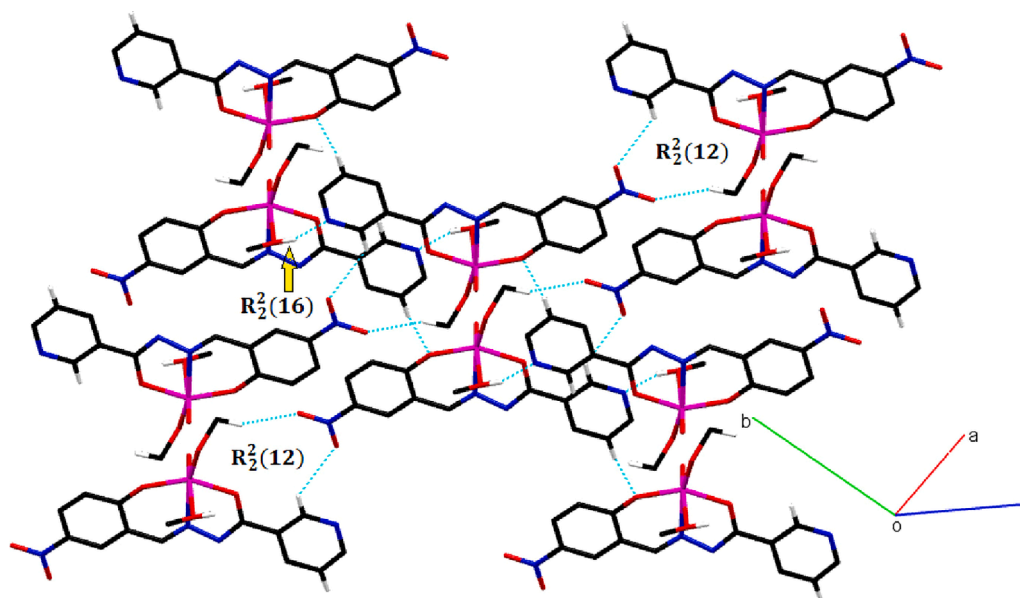


**Fig. 2.** Packing diagram of **VOL**. Only selected H-atoms are shown for clarity.

Hirshfeld surface analysis which gives useful information about the non-covalent interactions of molecules with neighboring ones which are responsible for crystal packing [79]. These intermolecular interactions can be displayed on HS by color coding and by plotting the HS over $d_{norm}$ [80-83]. The atomic contacts having distance shorter, equal and longer than summation of van der Waals radii are represented by red, white and blue regions on HS, respectively. Bright red spot-on HS near the *N*-atom of the pyridine ring is obvious for both compounds indicates that this *N*-atom is involved in strong intermolecular interaction as shown in Fig. 6a and 6b. On HS of **VOL**, bright red spot is present near OH of methanol (O5/H5A/C15) indicating that this is involved in H-bonding whereas on HS of **MoO$_2$L**, bright red spot is present near OH of ethanol (O5/H5A/C14/C15) indicating that this is involved in H-bonding as displayed in

Fig. 6b.

For both compounds, absence of red spots on HS near the *N*-atom of the nitro group and near imine *N*-atom indicate that these atoms are not engaged in H-bonding. Light red spots are present on the HS near the atoms which are involved in comparably weak bonding of type C—H…O for both compounds.

2D fingerprint plot is an efficient way for quantitative analysis of intermolecular interactions [84-89]. Fingerprint plots empower us to compute the percentage contribution of each interatomic contact in crystal packing. 2D plot for overall interactions for **VOL** and **MoO$_2$L** are displayed in Fig. 7a and 8a, respectively, in which all the interatomic contacts are determined including the reciprocal contacts as well. $d_e$ and $d_i$ represent distance from the HS to the nearest nucleus outside and
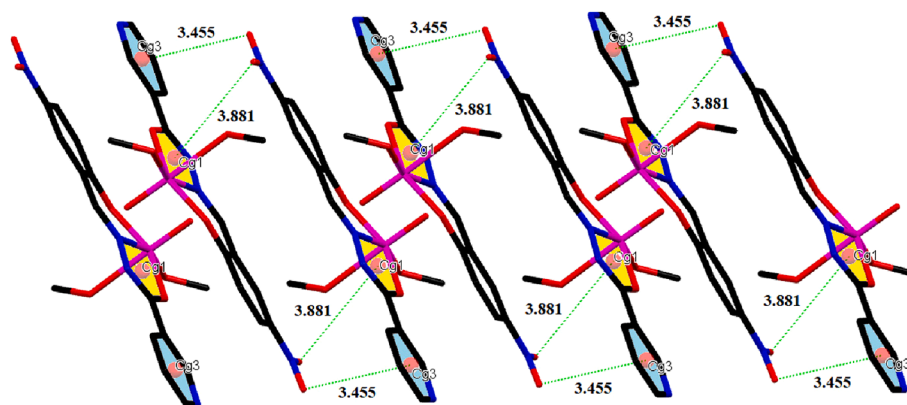
**Fig. 3.** Graphical representation of N—O…π interaction for **VOL**. Distances are measured in Å.

**Table 2**
Hydrogen-bond geometry (Å, °) for **VOL** and **MoO₂L**.

| | *D—H⋯A* | *D—H* | *H⋯A* | *D⋯A* | *D—H⋯A* |
|---|---|---|---|---|---|
| **VOL** | O5—H5A⋯N3[i] | 0.91 (3) | 1.91 (3) | 2.795 (3) | 163 (3) |
| | C10—H10⋯O6[ii] | 0.93 | 2.62 | 3.291 (4) | 129 |
| | C12—H12⋯O1[iii] | 0.93 | 2.62 | 3.525 (3) | 165 |
| | C14—H14A⋯O7[ii] | 0.96 | 2.46 | 3.356 (4) | 156 |
| | *Y—X⋯Cg* | *Y—X* | *X⋯Cg* | *Y⋯Cg* | *Y—X⋯Cg* |
| | N4—O6⋯Cg1[iv] | 1.2135 (4) | 3.881 (3) | 4.225(3) | 98.05(2) |
| | N4—O7⋯Cg3[iv] | 1.2332 (3) | 3.455 (4) | 3.852(4) | 99.3(2) |
| **MoO₂L** | O5—H5A⋯N3[v] | 0.86 (1) | 1.83 (2) | 2.685 (7) | 180 (7) |
| | C5—H5⋯O4[vi] | 0.93 | 2.61 | 3.389 (8) | 142 |
| | C7—H7⋯O4[vi] | 0.93 | 2.42 | 3.271 (6) | 152 |
| | C14A—H14A⋯O4 | 0.97 | 2.57 | 3.090 (11) | 114 |
| | C14B—H14C⋯O2 | 0.97 | 2.54 | 3.11 (4) | 117 |

**Symmetry codes:** $-x + 1$, $-y$, $-z + 1$; (ii) $x + 1$, $y$, $z + 1$; (iii) $\times$ ,$y - 1$, $z$; (iv) $-x$, $-y$, $-z$; (v) $-x + 1/2$, $y + 1/2$, $z + 1/2$; (vi) $x - 1/2$, $-y + 1/2$, $z$. Cg1 and Cg3 are the centroid of (C8/N1/N2/O2/V1), (C9-C13/N3) rings, respectively

**Table 3**
The selected experimental and calculated bond lengths (Å) and bond angles (°) of **VOL** and **MoO₂L** complexes.

| Bond length | Exp. | Calc. | Angle | Exp. | Calc. |
|---|---|---|---|---|---|
| **VOL** | | | | | |
| V(1)–O(1) | 1.874(2) | 1.873 | O(4)–V(1)–O(3) | 102.00(12) | 104.02 |
| V(1)–O(2) | 1.960(2) | 1.941 | O(4)–V(1)–O(1) | 103.09(8) | 101.33 |
| V(1)–O(3) | 1.587(2) | 1.568 | O(3)–V(1)–O(1) | 100.45(12) | 102.42 |
| V(1)–O(4) | 1.774(2) | 1.774 | O(4)–V(1)–O(2) | 92.52(8) | 93.75 |
| V(1)–O(5) | 2.330(2) | 2.551 | O(3)–V(1)–O(2) | 97.49(11) | 101.59 |
| V(1)–N(1) | 2.136(2) | 2.159 | O(1)–V(1)–O(2) | 153.09(9) | 147.48 |
| N(1)–C(7) | 1.285(3) | 1.288 | O(4)–V(1)–N(1) | 159.54(9) | 158.32 |
| N(1)–N(2) | 1.399(3) | 1.371 | O(3)–V(1)–N(1) | 95.51(10) | 95.80 |
| C(1)–O(1) | 1.327(3) | 1.312 | O(1)–V(1)–N(1) | 83.81(8) | 82.57 |
| C(8)–O(2) | 1.312(3) | 1.309 | O(2)–V(1)–N(1) | 74.61(8) | 73.45 |
| **MoO₂L** | | | | | |
| Mo(1)–O(1) | 1.943(4) | 1.969 | O(1)–Mo(1)–O(2) | 148.92(15) | 144.03 |
| Mo(1)–O(2) | 2.010(4) | 1.998 | O(1)–Mo(1)–O(3) | 97.8(2) | 100.81 |
| Mo(1)–O(3) | 1.679(4) | 1.686 | O(1)–Mo(1)–O(4) | 103.7(2) | 102.14 |
| Mo(1)–O(4) | 1.689(3) | 1.698 | O(1)–Mo(1)–O(5) | 80.46(17) | 74.98 |
| Mo(1)–O(5) | 2.290(4) | 2.545 | O(3)–Mo(1)–O(5) | 169.96(17) | 170.95 |
| Mo(1)–N(1) | 2.254(4) | 2.294 | O(4)–Mo(1)–O(5) | 84.5(2) | 81.44 |
| N(2)–C(8) | 1.300(6) | 1.299 | O(1)–Mo(1)–N(1) | 80.64(15) | 79.40 |
| N(1)–N(2) | 1.383(6) | 1.372 | O(2)–Mo(1)–N(1) | 71.65(14) | 70.50 |
| C(1)–O(1) | 1.348(6) | 1.325 | O(3)–Mo(1)–N(1) | 92.45(17) | 95.88 |
| C(8)–O(2) | 1.325(5) | 1.32 | O(4)–Mo(1)–N(1) | 160.6(2) | 155.75 |

inside the HS, respectively. H…H interatomic contact is found to be the greatest contributor in crystal packing of **VOL** with percentage contribution of 36.1% (Fig. 7b), whereas O…H interatomic contact is found to be the greatest contributor in crystal packing for **MoO₂L** with percentage contribution of 40% (Fig. 8b). For **VOL**, irrespective to most significant contributor in crystal packing, the other interatomic contacts that contribute in crystal packing are O…H, C…H, N…H, C…C, O…C, N…C, O…N, N…N and O…O with percentage contribution of 31.3%, 10.9%, 5.9%, 4.2%, 3.9%, 3.7%, 2.1%, 1.4% and 0.5% as displayed in Fig. 7(c-k), respectively. In crystal packing of **MoO₂L**, in addition to O…H interatomic contact, the other interatomic contacts for crystal packing are H…H, N…H, C…H, N…C, O…O, O…C and O…N with percentage contribution of 28.5%, 8.1%, 7.4%, 6.9%, 3.7%, 2.1%, 2% and 1.2% as displayed in Fig. 8(c-j).

In order to investigate the interaction of an atom present inside the HS to all the atoms of molecules located in the surrounding of HS, 2D plots of corresponding HS are employed. It is found that H-atoms present inside the HS have stronger interaction with all the atoms of molecules located in the surrounding of HS as compared to other atoms present in HS for both compounds. Percentage contribution of H-ALL interaction is 57.8% (Fig. 9a) and 53.7% (Fig. 9b) for **VOL** and **MoO₂L**, respectively. Other such interactions are O-ALL, C-ALL and *N*-ALL with percentage contributions of 26.4%, 14.2%, 7.4% (Fig. 9a) for **VOL**, respectively and 24.9%, 14.4%, 7% (Fig. 9b) for **MoO₂L**, respectively.

Furthermore, the interaction of all the atoms present inside the HS to an atom located in the surrounding of HS is employed by utilizing HS and 2D plots. ALL-H interaction is found to be the most important contributor in crystal packing for both compounds with percentage contribution of 62.3% (Fig. 10a) and 59.4% (Fig. 10b) for **VOL** and **MoO₂L**, respectively. Other such interactions are ALL-O, ALL-C and ALL-N with percentage contributions of 18%, 12.4%, 7.1% (Fig. 10a) for **VOL**, respectively and 21.7%, 12.9%, 6% (Fig. 10b) for **MoO₂L**, respectively.

*3.3. Optimized structural parameters*

DFT methods were used to determine and analyze the structure of ligand and its complexes at the B3LYP/Def2-TZVP level of theory in the gas phase. The optimized structures of compounds are presented in Fig. 11 and selected experimental and theoretical structural parameters including bond lengths and bond angles of the complexes are gathered in Table 3. It is obvious Table 3 that the theoretical data are quite comparable to the experimental findings. The differences between the theoretical and experimental values may be emanated from this fact that the experimental data belong to the solid state, while the calculated values describe a single molecule in the gaseous state. In accordance with X-ray crystal structures, the coordination of nitrogen and oxygen atoms to the metal center of V and Mo complexes in the gas phase exhibit
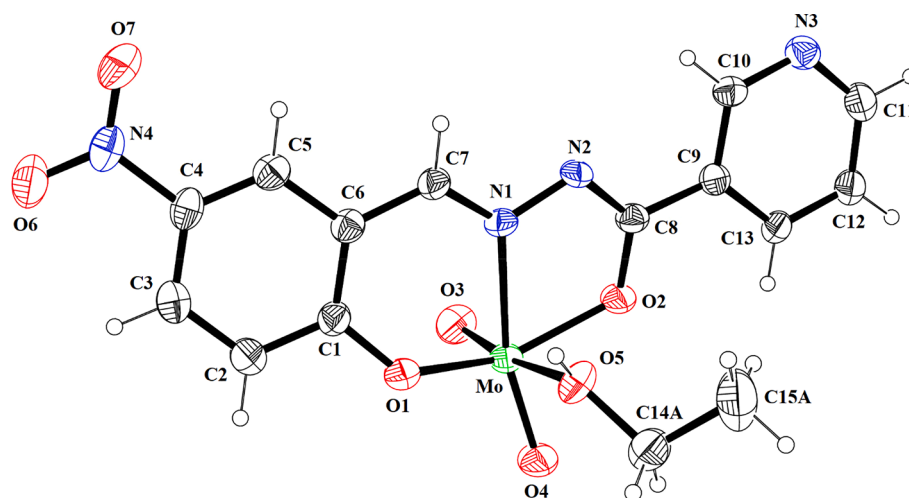
**Fig. 4.** ORTEP diagram of **MoO₂L** drawn at probability level of 30%. H-atoms are shown by small circles of arbitrary radii.
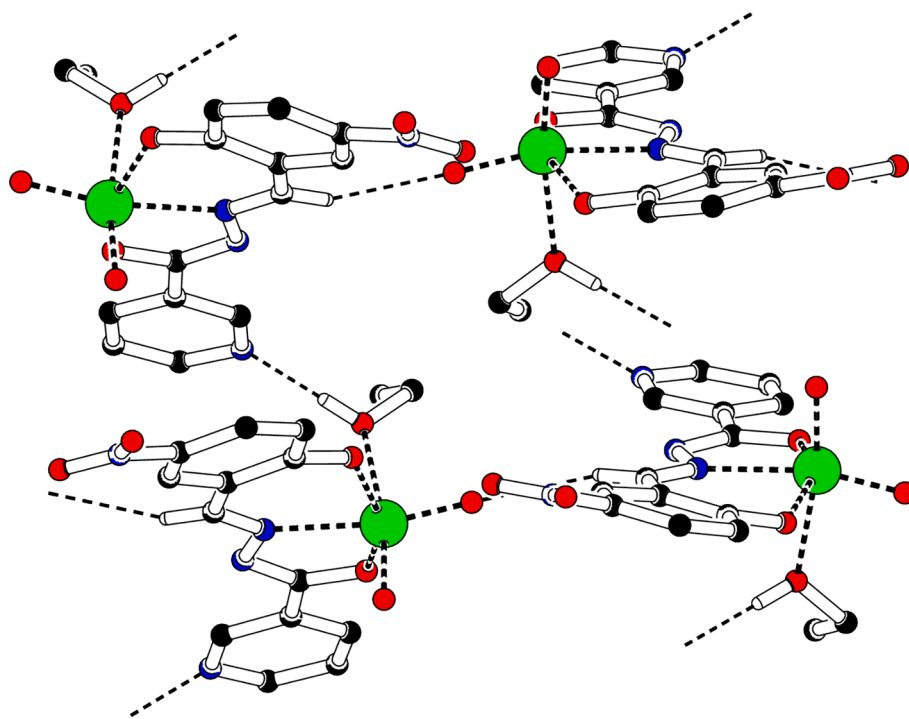


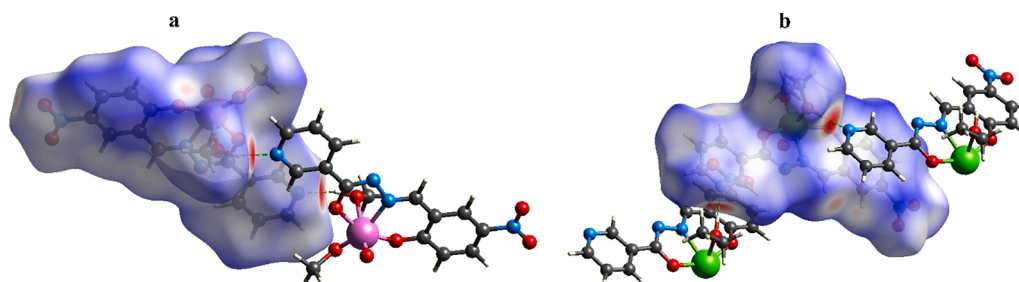**Fig. 5.** Packing diagram of **MoO₂L**. Only selected H-atoms are shown for clarity.



**Fig. 6.** HS plotted over $d_{norm}$ (a) for **VOL** in the range −0.0574 to 1.3435 a.u (b) for **MoO₂L** in the range −0.0411 to 1.2326 a.u.
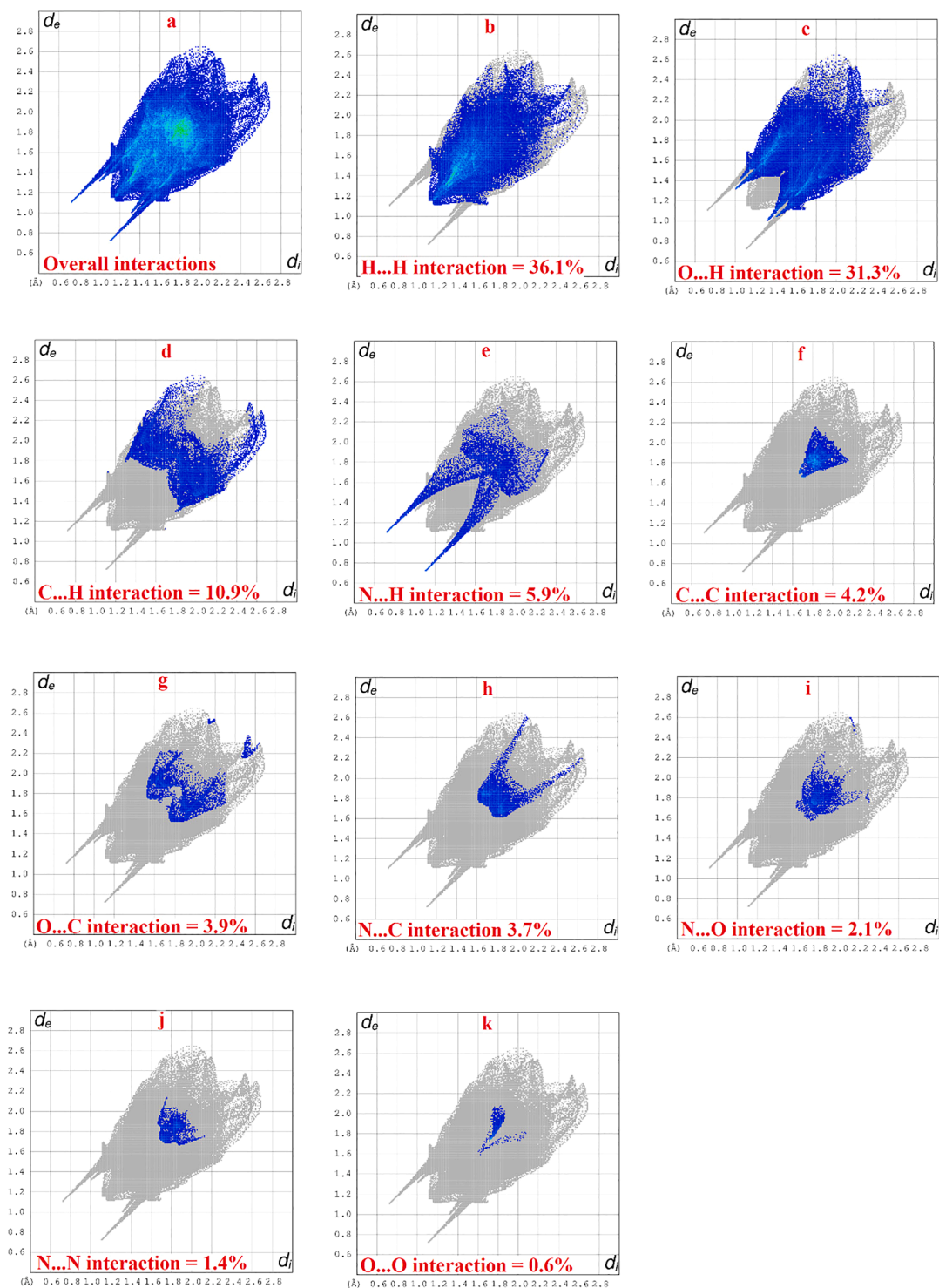
**Fig. 7.** 2D fingerprint plots for **VOL. (a)** for overall interactions, **(b-k)** for individual interactions.

the distorted octahedral geometry.

### 3.4. FT-IR spectra

The FT-IR spectra of the Schiff base ligand and its oxovanadium and dioxomolybdenum complexes are shown in Fig. 12. A careful comparison of the spectra of the synthesized compounds was carried out to look deeply into the sites of coordination of ligands with metals. The FT-IR spectrum of the ligand shows two bands in the region of 3302 and 1631 cm$^{-1}$ which correspond to the stretching vibrations of the $\nu$(NH)

and $\nu$(C=O). These bands disappear in the spectra of the complexes which is in accordance with the enolization of the amide functional group and succeeding the deprotonation to get attached with metal ions. The X-ray diffraction data also confirm the same mode of coordination of the ligand. The particular stretching vibration of azomethine group (–HC = N) in ligand appears at 1600 cm$^{-1}$ also shows a slight shift on complexation. New bands emerging at 1263 and 1313 cm$^{-1}$ are attributed to enolic $\nu$(C—O) moiety in molybdenum and vanadium complexes, respectively. The appearance of two new bands at 916 and 933 cm$^{-1}$ are assigned to symmetric and asymmetric stretching vibrations of the *cis-*
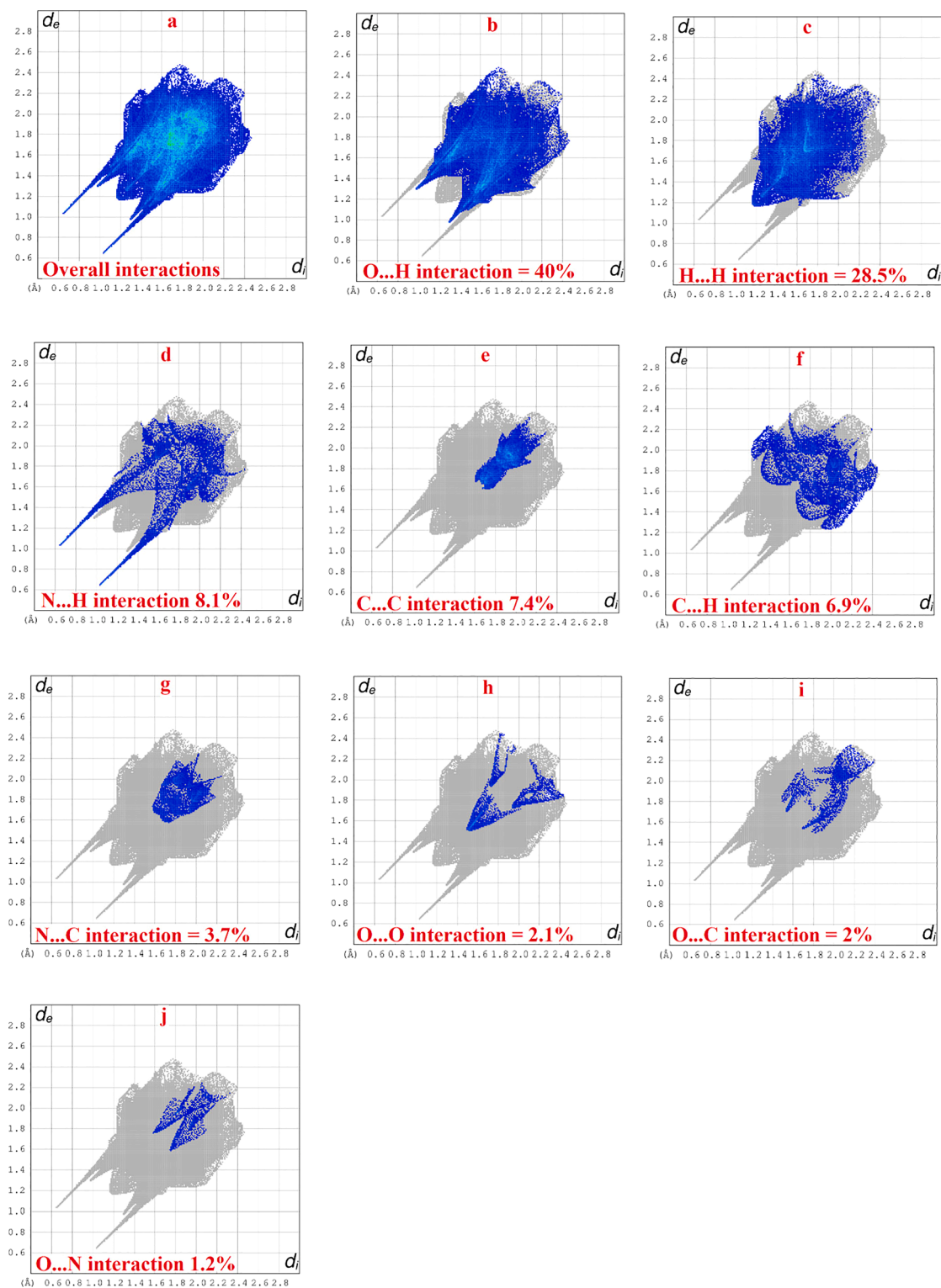
**Fig. 8.** 2D fingerprint plots for **MoO₂L**. **(a)** for overall interactions, **(b-j)** for individual interactions.

Mo(O)₂ moiety which are in accordance with similar structures reported previously in literature [90,91]. Similarly, oxovanadium complex also gives its characteristics peak of V = O at 918 cm⁻¹ which is very close to the values of similar oxovanadium Schiff base complexes already reported in literature [92-94]. In addition, some new M−O and M−N peaks are also visible at 597 & 476 cm⁻¹ for Mo complex and at 580 & 457 cm⁻¹ for V complex, respectively. These values are also in agreement to the similar reported complexes [92-95].

Typical selected experimental and calculated vibrational modes of the ligand and its oxovanadium and dioxomolybdenum complexes are listed in Table 4. Theoretical calculations exhibit good agreement with experimental results.

*3.5. ¹H NMR and ¹³C NMR spectra*

The ¹H and ¹³C NMR spectral data of the **H₂L**, **VOL** and **MoO₂L**
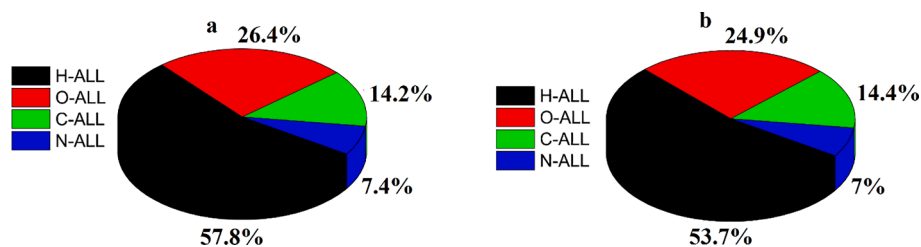
**Fig. 9.** Percentage contribution of interaction of an atom present inside HS to all the atoms located in the surrounding of HS (a) for **VOL**, (b) for **MoO₂L**.
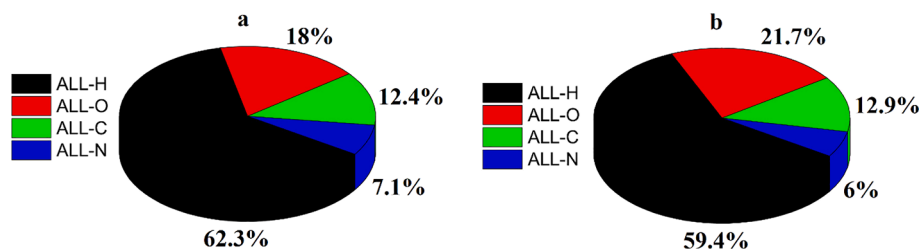


**Fig. 10.** Percentage contribution of interaction of all the atoms present inside HS to an atom located in the surrounding of HS (a) For **VOL**, (b) For **MoO₂L**.
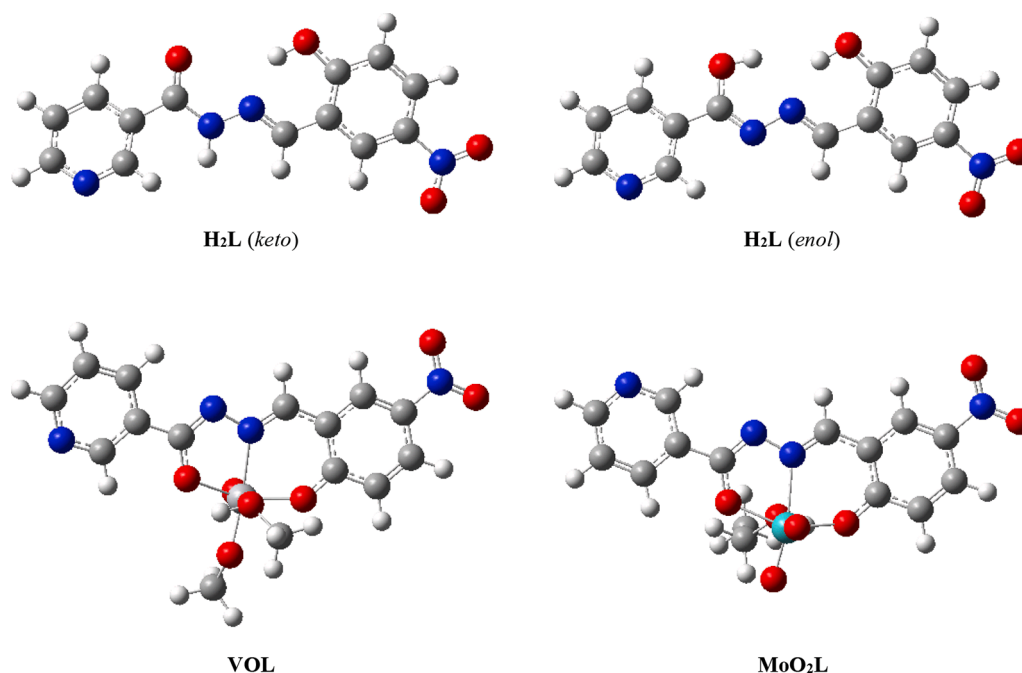


**Fig. 11.** Optimized structures of **H₂L** ligand (*keto* and *enol* form), **VOL** and **MoO₂L**.

complex recorded in DMSO-$d_6$ are presented in the experimental section and the spectra are shown in Figures S1-S6. Two signals, appearing at $\delta$ = 12.35 and 12.09 ppm in the $^1$H NMR spectrum of the ligand correspond to OH (phenolic) and NH protons, respectively, disappear upon reaction with V and Mo salts. This disappearance demonstrates that the phenolate and enolate oxygens are the sites of coordination of the ligand with the metals. This also ascertains the occurrence of keto-imine tautomerism upon complexation. Moreover, a singlet for azomethine proton (–HC = N) at $\delta$ = 8.71 ppm observed in the spectra of the ligand was shifted downfield at $\delta$ = 9.09 ppm in **VOL** and $\delta$ = 9.19 ppm in **MoO₂L** showing the deshielding due to the decrease in the electronic density upon the coordination of azomethine nitrogen with the metal ion. All the signals for aromatic protons in the $^1$H NMR spectrum of the ligand were observed in the expected range of $\delta$ = 7.08–9.09 ppm. There is a slight shift in the positions of aromatic protons signals of the ligand

upon complex formation ($\delta$ = 7.11–9.25 ppm in **VOL** and $\delta$ = 7.17–9.19 ppm in **MoO₂L**).

The $^{13}$C NMR spectra of the ligand and its V and Mo complexes are shown in Figures S4-S6. The signals for the carbonyl, phenolic and methine carbon in the V complex were observed at $\delta$ = 167.8, 158.2 and 155.9 ppm, respectively and in the Mo complex were observed at $\delta$ = 167.8, 163.9 and 156.0 ppm, respectively. The chemical shift values of the carbons present in vicinity of the coordinating atoms (i.e., C8, C1 and C7) showed appreciable change in their position due to coordination-induced shifts confirming the association of these functionalities in coordination. The other aromatic carbons of ligand and its complexes appeared in their respective regions according to the literature. Hence, $^{13}$C NMR spectra also support the conclusions derived from $^1$H NMR spectral data. The experimental and calculated $^1$H and $^{13}$C NMR chemical shift values of the ligand and complexes are given in Table 5.
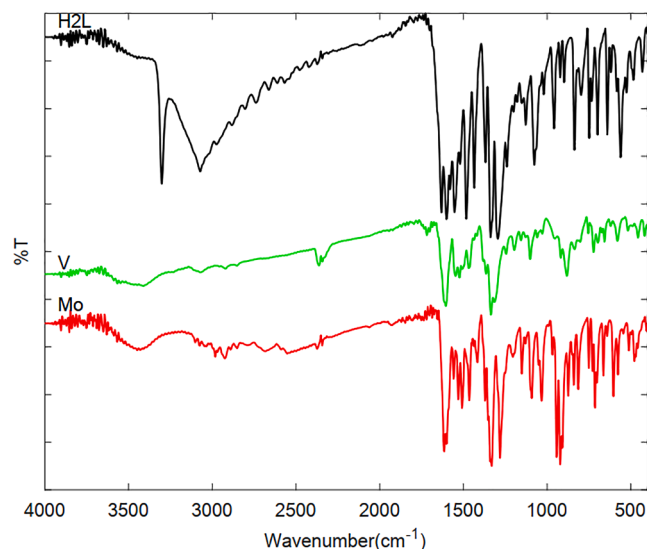
**Fig. 12.** FT-IR spectra of the ligand and its V and Mo complexes.

### 3.6. Mulliken atomic charges distribution

The calculated Mulliken charges for ligand and its oxovanadium and dioxomolybdenum complexes are listed in Table 6. The Mulliken charges at the central atoms are $+1.034e$ for V complex and $+1.477e$ for Mo complex. The charges on the metal atoms are considerably lower than the formal charges, $5+$ and $6+$ for vanadium and molybdenum, respectively, which indicate that the significant amount of charge density is transferred from the ligand to the metal atoms. Also, the highest charge density in the ligand was found on C1 and C8, while after the complexation, charge density on C1 in the gas phase increases from 0.204 to 0.360 and 0.397, and charge density on C8 in the gas phase increases from 0.290 to 0.355 and 0.429 in the **VOL** and **MoO₂L** complexes, respectively.

### 3.7. Electronic properties

In order to acquire the electronic distribution of frontier orbitals, the highest occupied molecular orbital (HOMO) and the lowest unoccupied molecular orbital (LUMO) energy levels of the ligand and its complexes, were calculated at B3LYP/Def2-TZVP level of theory. The results are presented in Fig. 13 while the HOMO and LUMO orbital energies and
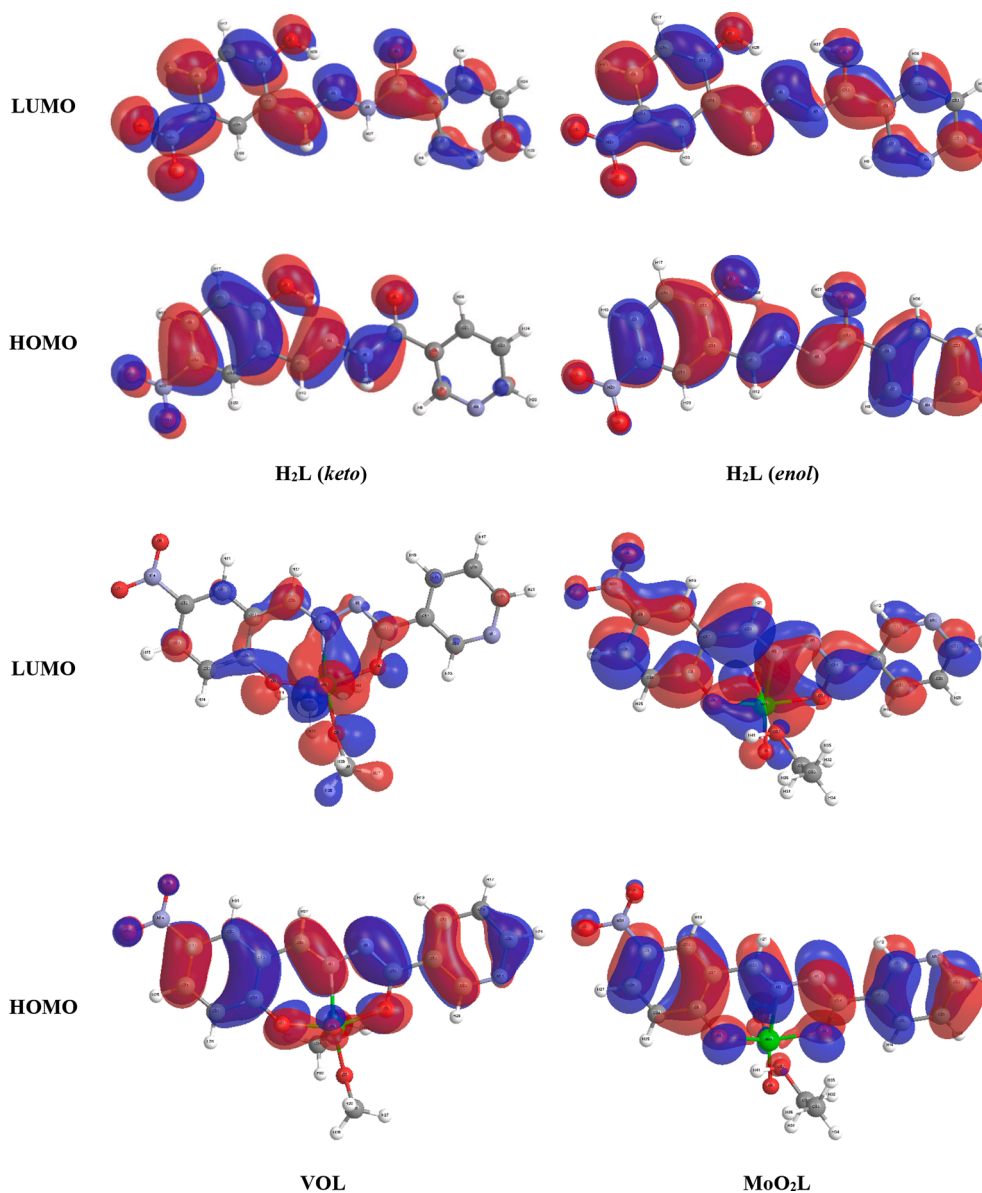
**Table 4**
Selected experimental and calculated FT-IR frequencies (cm$^{-1}$) of the **H₂L** ligand, **VOL** and **MoO₂L** complexes.

| Assignment | H₂L | | | VOL | | | MoO₂L | | |
|---|---|---|---|---|---|---|---|---|---|
| | Exp. | Calc.[a] | Relative error (%)[b] | Exp. | Calc.[a] | Relative error (%)[b] | Exp. | Calc.[a] | Relative error (%)[b] |
| –HC = N | 1600 | 1617 | 1.06 | 1604 | 1607 | 0.19 | 1612 | 1610 | −0.12 |
| C—O | 1294 | 1279 | −1.16 | 1313 | 1277 | −2.74 | 1263 | 1255 | −0.63 |
| M—O | – | – | | 580 | 581 | 0.17 | 597 | 596 | −0.17 |
| M—N | – | – | | 457 | 466 | 1.97 | 476 | 477 | 0.21 |

[a] Scaling factor, 0.965 [96].
[b] Relative error (%) = $(X^{Calc} - X^{Exp})*100/X^{Exp}$.

**Table 5**
Experimental and calculated $^1$H and $^{13}$C NMR shift values of **H₂L** ligand and its complexes (ppm).

| Atom | $^1$H NMR | | | | | | Atom | $^{13}$C NMR | | | | | |
|---|---|---|---|---|---|---|---|---|---|---|---|---|---|
| | H₂L | | VOL | | MoO₂L | | | H₂L | | VOL | | MoO₂L | |
| | Exp. | Calc. | Exp. | Calc. | Exp. | Calc. | | Exp. | Calc. | Exp. | Calc. | Exp. | Calc. |
| OH | 12.35 | 12.97 | – | – | – | – | C1 | 162.5 | 175.9 | 158.2 | 179.0 | 163.9 | 176.2 |
| NH | 12.09 | 9.33 | – | – | – | – | C8 | 161.6 | 169.4 | 167.8 | 180.3 | 167.8 | 178.3 |
| CH(10) | 9.09 | 9.31 | 9.25 | 9.51 | 9.18 | 9.92 | C11 | 152.5 | 161.7 | 155.9 | 161.1 | 152.7 | 161.2 |
| CH(11) | 8.77 | 9.17 | 8.87 | 9.10 | 8.81 | 9.11 | C10 | 148.6 | 154.5 | 149.0 | 158.0 | 148.9 | 158.8 |
| HC = N | 8.71 | 8.56 | 9.09 | 8.97 | 9.19 | 9.08 | C7 | 144.6 | 153.7 | 152.7 | 159.6 | 156.0 | 163.5 |
| CH(5) | 8.57 | 8.74 | 7.98 | 8.95 | 8.82 | 8.94 | C4 | 139.9 | 148.0 | 135.7 | 148.4 | 140.9 | 149.8 |
| CH(13) | 8.28 | 8.67 | 8.42 | 8.94 | 8.34 | 8.61 | C13 | 135.4 | 144.8 | 134.5 | 144.0 | 135.6 | 143.7 |
| CH(3) | 8.14 | 8.70 | 7.69 | 8.84 | 8.34 | 8.82 | C9 | 128.5 | 136.6 | 124.9 | 133.2 | 125.7 | 132.6 |
| CH(12) | 7.57 | 7.83 | 7.65 | 7.73 | 7.58 | 7.76 | C5 | 126.6 | 136.4 | 133.1 | 138.7 | 130.5 | 139.4 |
| CH(2) | 7.08 | 7.36 | 7.11 | 7.26 | 7.17 | 7.30 | C3 | 123.6 | 135.9 | 126.1 | 138.1 | 129.6 | 138.8 |
| | | | | | | | C12 | 119.9 | 130.7 | 124.1 | 130.0 | 124.0 | 130.0 |
| | | | | | | | C6 | 117.0 | 124.8 | 121.5 | 127.5 | 120.2 | 127.1 |
| | | | | | | | C2 | 116.7 | 123.1 | 120.7 | 123.3 | 120.1 | 125.5 |

**Table 6**
The Mulliken atomic charges of the **H₂L** ligand, **VOL** and **MoO₂L** complexes.

| Atom | H₂L | VOL | MoO₂L | Atom | H₂L | VOL | MoO₂L | Atom | H₂L | VOL | MoO₂L |
|---|---|---|---|---|---|---|---|---|---|---|---|
| M1 | – | 1.034 | 1.477 | N2 | −0.176 | −0.249 | −0.244 | C7 | −0.019 | −0.074 | −0.034 |
| O1 | −0.359 | −0.500 | −0.571 | N3 | −0.207 | −0.204 | −0.200 | C8 | 0.290 | 0.397 | 0.429 |
| O2 | −0.325 | −0.492 | −0.538 | N4 | 0.426 | 0.425 | 0.428 | C9 | 0.056 | 0.033 | 0.015 |
| O3 | −0.317 | −0.435 | −0.530 | C1 | 0.204 | 0.360 | 0.355 | C10 | −0.100 | −0.151 | −0.072 |
| O4 | −0.323 | −0.432 | −0.498 | C2 | −0.170 | −0.155 | −0.158 | C11 | −0.024 | −0.096 | −0.020 |
| O5 | – | −0.441 | −0.451 | C3 | −0.131 | −0.148 | −0.141 | C12 | −0.082 | −0.024 | −0.095 |
| O6 | – | −0.317 | −0.312 | C4 | 0.028 | 0.053 | 0.050 | C13 | −0.150 | −0.074 | −0.146 |
| O7 | – | −0.318 | −0.313 | C5 | −0.212 | −0.244 | −0.236 | C14 | – | −0.155 | −0.001 |
| N1 | −0.159 | 0.066 | −0.053 | C6 | 0.116 | 0.137 | 0.131 | C15 | – | −0.154 | −0.326 |

**Fig. 13.** DFT-optimized frontier molecular orbitals for **H₂L** ligand, **VOL** and **MoO₂L** complexes.

**Table 7**
The HOMO and LUMO orbital energies and the energy gaps of the **H₂L** ligand, **VOL** and **MoO₂L** complexes.

| E (eV) | H₂L (*keto*) | H₂L (*enol*) | VOL | MoO₂L |
|---|---|---|---|---|
| $E_{HOMO}$ | −6.922 | −6.878 | −6.627 | −6.943 |
| $E_{LUMO}$ | −2.672 | −2.837 | −3.320 | −3.255 |
| *Energy gap | 4.250 | 4.041 | 3.307 | 3.688 |

* $E_g = E_{LUMO} - E_{HOMO}$.

energy gaps (ΔE) for the compounds are given in Table 7. As shown in Table 7, the energy gaps for the **H₂L** (keto), **H₂L** (enol), **VOL** and **MoO₂L** were found to be 4.250, 4.041, 3.307 and 3.688 eV, respectively. The energy gap of **H₂L** (keto) is slightly greater than **H₂L** (enol), which can be attributed to higher stability of keto tautomeric form of the ligand.

To investigate the linkage between molecular structure and physicochemical property of molecules, the molecular electrostatic potential (MEP) can be used. The MEP can show electrophilic sites (positive regions) and nucleophilic sites (negative regions) of the molecule based on their electrostatic potentials which are illustrated by blue and red colors,

respectively. The MEP diagrams and values of electrostatic potentials of ligand and its V and Mo complexes are shown in Fig. 14. There is a significant difference between electrostatic potential values of enol and keto forms of **H₂L** ligand. In keto form, the more negative site is located between phenolic and carbonylic oxygen atoms, with electrostatic values of ~ 61 kcal.mol⁻¹, while in enol form, the blue color can be seen between two hydroxyl groups which means this area has the positive electrostatic potential (~46 kcal.mol⁻¹). In the oxovanadium and dioxomolybdenum complexes with electrostatic potential values of ~ 34 and ~ 54 kcal.mol⁻¹, respectively, the metal atom is the center of positive potential represented by blue color which means it is a good candidate for the attack by a nucleophile. These results are in agreement with the Mulliken atomic charges (Table 6).

The sum of the electronic and the zero-point energy ($E^{ZPE}$), enthalpy (H), and Gibbs free energy of both enol and keto forms of **H₂L** Schiff base ligand are presented in Table 8. The data showed that keto form is more stable in both, gas and solution phases. This result is consistent with the findings from the molecular electrostatic potentials (MEP) values and from the comparison of energy gaps between HOMO and LUMO of keto and enol tautomeric forms of the ligand (See Figs. 13 and 14).
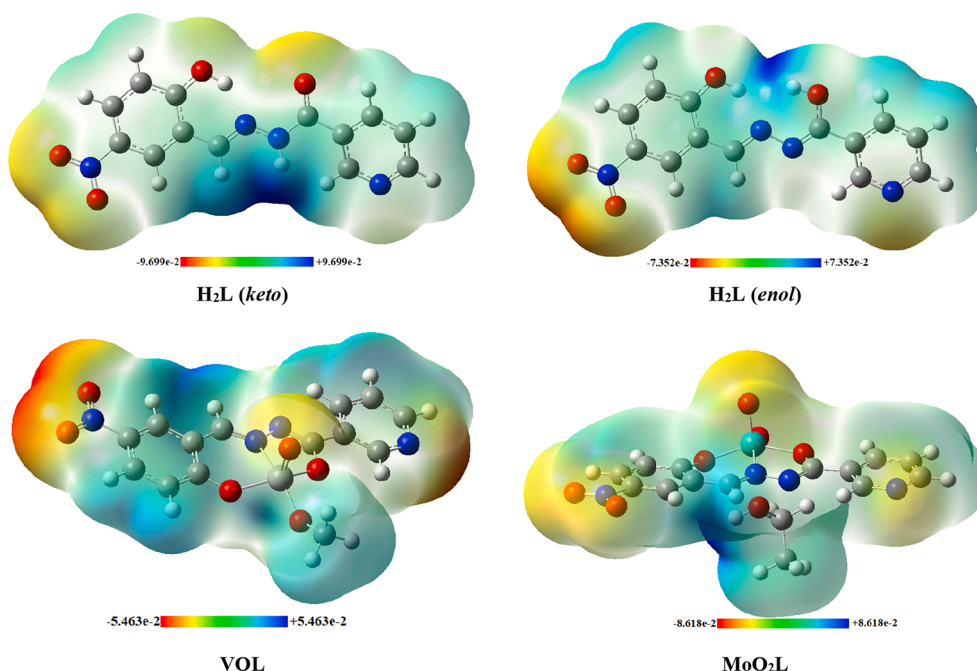
**Fig. 14.** Molecular electrostatic potential (MEP) for **H₂L** ligand, **VOL** and **MoO₂L** complexes with color range along with scale.

**Table 8**
Sum of the electronic and the zero-point energy ($E^{ZPE}$), enthalpy (H), and Gibbs free energy of the **H₂L** ligand. All values are listed in Hartree unit.[a]

|  | **H₂L (keto)** | | **H₂L (enol)** | |
|---|---|---|---|---|
|  | **Gas phase** | **Solution phase** | **Gas phase** | **Solution phase** |
| $E^{ZPE}$ | −1021.373 | −1021.394 | −1021.365 | −1021.380 |
| H | −1021.355 | −1021.376 | −1021.347 | −1021.362 |
| G | −1021.421 | −1021.442 | −1021.412 | −1021.429 |

[a] 1 Hartree = 627.5095 kcal.mol$^{-1}$.

**Table 9**
Effect of solvent on oxidation of 4-chlorobenzyl alcohol with UHP catalyzed by **VOL** and **MoO₂L** complexes.[a]

| Entry | Solvent | VOL Yield (%) after 10 min.[b] | MoO₂L Yield (%) after 2 h[b] |
|---|---|---|---|
| 1 | $CH_3CH_2OH$ | 50 | 35 |
| 2 | $CH_3CN$ | 90, Trace[c], 55[d], 70[e], 82[f] | 88, Trace[c], 60[d], 73[e], 80[f] |
| 3 | $ClCH_2CH_2Cl$ | 30 | 20 |
| 4 | $CH_3COCH_3$ | 80 | 50 |
| 5 | $CHCl_3$ | 30 | 20 |
| 6 | $CCl_4$ | 5 | 0 |
| 7 | $CH_2Cl_2$ | 0 | 0 |

[a] Reaction conditions: 4-chlorobenzyl alcohol (1 mmol), UHP (2 mmol), catalyst (0.006 mmol), solvent (10 mL) under reflux conditions.
[b] Isolated yield.
[c] The reaction was performed at room temperature.
[d] The reaction was performed at 40 °C.
[e] The reaction was performed at 60 °C.
[f] The reaction was performed at 70 °C.

**Table 10**
Effect of oxidant on oxidation of 4-chlorobenzyl alcohol catalyzed by **VOL** and **MoO₂L** complexes.[a]

| Entry | Oxidant | VOL Yield (%) after 10 min.[b] | MoO₂L Yield (%) after 2 h[b] |
|---|---|---|---|
| 1 | No oxidant | 0 | 0 |
| 2 | $NaIO_4$ | 15 | 20 |
| 3 | $H_2O_2$ | 75 | 70 |
| 4 | UHP | 90 | 88 |
| 5 | $(Bu)_4NIO_4$ | 5 | 0 |
| 6 | *tert*-BuOOH | 50 | 40 |

[a] Reaction conditions: 4-chlorobenzyl alcohol (1 mmol), oxidant (2 mmol), catalyst (0.006 mmol), $CH_3CN$ (10 mL) under reflux conditions.
[b] Isolated yield.

**Table 11**
Optimization of catalyst amount in oxidation of 4-chlorobenzyl alcohol with UHP catalyzed by **VOL** and **MoO₂L** complexes[a].
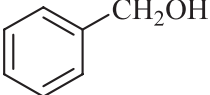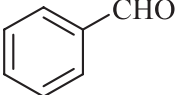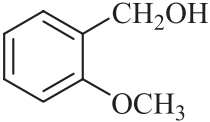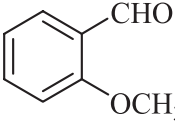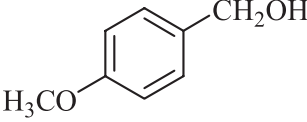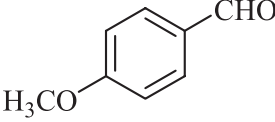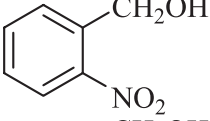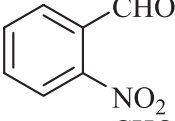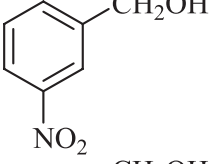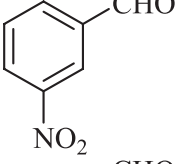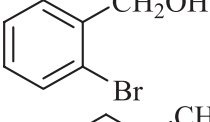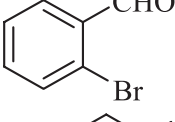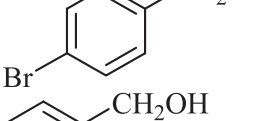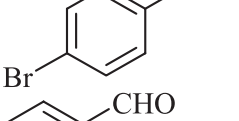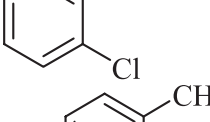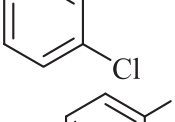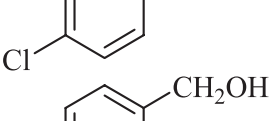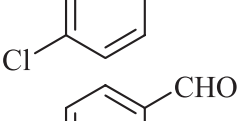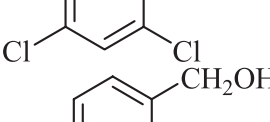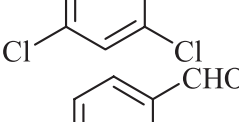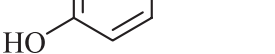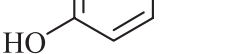
| Entry | Catalyst amount (mmol) | VOL Yield (%) after 10 min.[b] | MoO₂L Yield (%) after 2 h[b] |
|---|---|---|---|
| 1 | No catalyst | 0 | 0 |
| 2 | 0.002 | 40 | 35 |
| 3 | 0.004 | 80 | 75 |
| 4 | 0.006 | 90 | 88 |
| 5 | 0.008 | 91 | 90 |

[a] Reaction conditions: Benzyl alcohol (1 mmol), UHP (2 mmol), catalyst, $CH_3CN$ (10 mL) under reflux conditions
[b] Isolated yield

### 3.8. Catalytic activity studies

Vanadium and molybdenum complexes have been used as catalysts for various organic reactions [74,97]. With comparison to reported species, the present two complexes have excellent performance. Catalytic abilities of **VOL** and **MoO₂L** complexes have been studied in the oxidation reactions of benzylic alcohols.

The oxidation of 4-chlorobenzyl alcohol using urea hydrogen peroxide (UHP), which cannot proceed in the absence of catalyst under mild and reflux conditions, was used as a model reaction. To find the optimum reaction conditions, the influence of different factors that may affect the conversion of the reaction was investigated. A systematic examination of oxidation of 4-chlorobenzyl alcohol in various solvents such as ethanol, acetonitrile, acetone, 1,2-dichloroethane, dichloromethane, chloroform and carbon tetrachloride were carried out in the presence of 0.006 mmol of V/Mo complexes catalysts. Keeping in mind the yield and reaction rate, acetonitrile was found to be the best solvent,

**Table 12**

Selective oxidation of benzylic alcohols to benzaldehydes with UHP catalyzed by **VOL** and **MoO$_2$L** complexes.[a]

| Entry | Alcohol | Aldehyde[b] | VOL complex | | | MoO$_2$L complex | | |
|---|---|---|---|---|---|---|---|---|
| | | | Time (min) | Yield (%)[c] | TOF (h$^{-1}$)[d] | Time (h) | Yield (%)[c] | TOF (h$^{-1}$)[d] |
| 1 |  CH$_2$OH |  CHO | 10 | 93 | 930 | 2 | 91 | 76 |
| 2 | CH$_2$OH, OCH$_3$ | CHO, OCH$_3$ | 15 | 95 | 633 | 2 | 89 | 74 |
| 3 | CH$_2$OH, H$_3$CO | CHO, H$_3$CO | 10 | 91 | 910 | 2 | 91 | 76 |
| 4 | CH$_2$OH, NO$_2$ | CHO, NO$_2$ | 10 | 90 | 900 | 2 | 88 | 73 |
| 5 | CH$_2$OH, NO$_2$ | CHO, NO$_2$ | 15 | 91 | 607 | 2.5 | 90 | 60 |
| 6 | CH$_2$OH, Br | CHO, Br | 10 | 93 | 930 | 2 | 93 | 78 |
| 7 | CH$_2$OH, Br | CHO, Br | 12 | 92 | 767 | 2 | 89 | 74 |
| 8 | CH$_2$OH, Cl | CHO, Cl | 10 | 91 | 910 | 2 | 93 | 78 |
| 9 | CH$_2$OH, Cl | CHO, Cl | 10 | 90 | 900 | 2 | 88 | 73 |
| 10 | CH$_2$OH, Cl, Cl | CHO, Cl, Cl | 15 | 96 | 640 | 3 | 94 | 52 |
| 11 | CH$_2$OH, HO | CHO, HO | 10 | 91 | 910 | 2 | 89 | 74 |

[d] TOF = (mmol of product)/[(mmol of catalyst) × (time)].
[a] Reaction conditions: Benzylic alcohol (1 mmol), UHP (2 mmol), catalyst (0.006 mmol), CH$_3$CN (10 mL) under reflux conditions.
[b] All products were identified by comparison of their physical and spectral data with those of authentic samples.
[c] Isolated yield.

which under reflux conditions, can complete the reaction in the desired period of time (Table 9).

Considering our observations, higher reaction temperature has an overall benefit to achieve the better yield and hence the reactions under reflux conditions can be completed within 10 min. for **VOL** complex and 2 h for **MoO$_2$L** complex. Similar findings about the association of higher reaction temperature with improved yields have also been reported

earlier [98].

Among the screened oxidants, including NaIO$_4$, H$_2$O$_2$, UHP, Bu$_4$NIO$_4$ and *tert*-BuOOH for the oxidation of 4-chlorobenzyl alcohol using **VOL** and **MoO$_2$L** complexes, UHP was found to be the best source of oxygen (Table 10).

Different amounts of the catalyst have been used for the oxidation of 4-chlorobenzyl alcohol with UHP in acetonitrile under reflux conditions
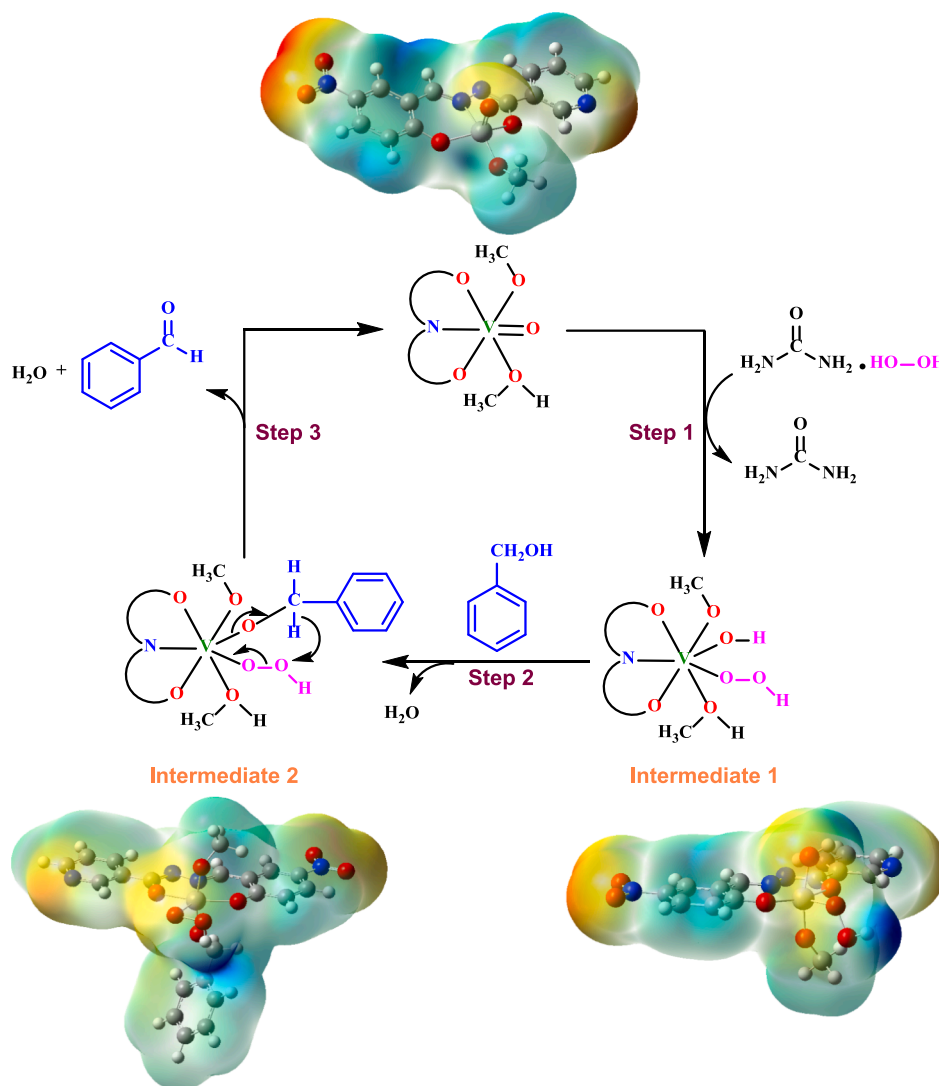
**Scheme 3.** Plausible mechanism for oxidation of benzyl alcohol with UHP catalyzed by **VOL** complex.

(Table 11). It was observed that the subjected oxidation process requires 10 min. for completion by using 0.006 mmol of the V complex catalyst and an increase in this amount did not noticeably effect on the reaction rate and product yield. The optimized amount of the Mo complex catalyst was the same in this reaction, with the exception of longer reaction time (2 h).

After investigation of the optimal conditions, we have explored that the substrate scope of the newly developed V and Mo complexes as catalyst, under the optimum condition, for the selective oxidation of a wide range of benzylic alcohols carrying electron-donating and electron-withdrawing groups to their corresponding substituted benzaldehydes. The results are summarized in Table 12.

The chemoselectivity of the method was notable. The oxidative hydroxyl group was tolerated under the influence of this catalytic system and the corresponding aldehyde was obtained in 100% selectivity. The beauty of the protocol is that no overoxidation to benzoic acid took place with all the studied substrates. In addition, in the case of 4-hydroxybenzyl alcohol, the benzyl hydroxyl group is selectively oxidized and while the phenolic hydroxyl group does not react at all. In order to further clarify the efficiency of the catalysts, the turnover frequency (TOF) is also calculated and given in Table 12.

Based on experimental results and related literature [99], for the oxidation reactions mediated by oxometal complexes, a plausible mechanism for oxidation of benzyl alcohol with UHP catalyzed by **VOL**

**Table 13**
Sum of the electronic and the zero-point energy ($E^{ZPE}$), enthalpy (H), and Gibbs free energy of all the materials involved in the oxidation of benzyl alcohol catalyzed by **VOL** complex in the refluxed acetonitrile. All values are listed in Hartree unit.[a]

| Compound | $E^{ZPE}$ | H | G |
|---|---|---|---|
| VOL | −2154.792 | −2154.760 | −2154.861 |
| Intermediate 1 | −2306.365 | −2306.329 | −2306.440 |
| Intermediate 2 | −2576.708 | −2576.665 | −2576.794 |
| Benzyl alcohol | −346.786 | −346.775 | −346.826 |
| $H_2O_2$ | −151.599 | −151.594 | −151.627 |
| Benzaldehyde | −345.605 | −345.595 | −345.643 |
| $H_2O$ | −76.449 | −76.445 | −76.471 |

[a] 1 Hartree = 627.5095 kcal.mol$^{-1}$.

Schiff base complex is proposed in Scheme 3. The catalyst, **VOL** which is an oxovanadium(V) complex, is inactive as such in the oxidation process. As shown in the MEP diagram of **VOL** and also previously mentioned, the metal atom in the complex is electropositive and can be attacked by nucleophiles. Thus, the **VOL** complex reacts with a hydrogen peroxide molecule released from UHP to form the peroxovanadium species (Intermediate 1). The peroxovanadium is active in oxidation and after etherification of OH group in intermediate 1 by benzyl alcohol, intermediate 2 is produced. Finally, this intermediate

**Table 14**
The changes of the electronic and the zero-point energy ($\Delta E^{\mathrm{ZPE}}$), enthalpy ($\Delta H$), and Gibbs free energy ($\Delta G$) of all the reaction steps in the oxidation of benzyl alcohol catalyzed by **VOL** complex in the refluxed acetonitrile.

| | $\Delta E^{\mathrm{ZPE}}$ | | $\Delta H$ | | $\Delta G$ | |
|---|---|---|---|---|---|---|
| | Hartree | kcal. mol$^{-1}$ | Hartree | kcal. mol$^{-1}$ | Hartree | kcal. mol$^{-1}$ |
| Step 1 | 0.025 | 15.69 | 0.025 | 15.69 | 0.047 | 29.49 |
| Step 2 | −0.007 | −4.39 | −0.005 | −3.14 | 0.000 | 0.00 |
| Step 3 | −0.137 | −85.97 | −0.136 | −85.34 | −0.180 | −112.95 |

1 Hartree = 627.5095 kcal.mol$^{-1}$.

oxides benzyl alcohol to release one molecule of $H_2O$ to give benzaldehyde as the target product and regenerates the **VOL** Schiff base complex. A similar mechanism can also be drawn for the **MoO$_2$L** complex.

The sum of the electronic and the zero-point energy ($E^{\mathrm{ZPE}}$), enthalpy (H), and Gibbs free energy of all the materials involved in the selective oxidation of benzyl alcohol to benzaldehyde using UHP in the presence of **VOL** catalyst are listed in Table 13. By use of these values, $\Delta E^{\mathrm{ZPE}}$, $\Delta H$ and $\Delta G$ of all steps for this reaction were calculated (Table 14). As shown in Table 13, the first step of the reaction is endothermic ($\Delta G$ = 29.49 kcal.mol$^{-1}$) and can be carried out at 82 °C. The last step of the reaction is exothermic ($\Delta G$ = -112.95 kcal.mol$^{-1}$) and overall, the reaction is exothermic.

## 4. Conclusion

A new tridentate ONO-donor Schiff base ligand and its V(V) and Mo (VI) complexes were synthesized and characterized by various physicochemical techniques. The molecular structures of complexes were determined by single crystal X-ray crystallography. The coordination geometry around V and Mo metal centers was described better as distorted octahedral. Theoretical calculations of the Schiff base ligand and its V and Mo complexes were performed by DFT at B3LYP level with Def2-TZVP basis set and it was found that the theoretical data is in good agreement with the experimental results. The catalytic activity of the complexes was also performed by the oxidation of benzylic alcohols with UHP in acetonitrile. The present method offers various advantages such as high yield of the products and short interval of time for completion of reaction.

## 5. Authors' statement

We would like to make a statement about the author's main contribution: HK and PF synthesized all the compounds, and characterized them by different techniques; MFM and RBA designed the model and the computational framework and analyzed the data; HAR collected the single-crystal X-ray diffraction data, MA and MNT determined the structures and Hirshfeld surface analysis. HK and KSM wrote the manuscript with input from all authors. All authors discussed the results and commented on the manuscript.

## Declaration of Competing Interest

The authors declare that they have no known competing financial interests or personal relationships that could have appeared to influence the work reported in this paper.

## Acknowledgments

## Appendix A. Supplementary data

## References

[1] B. Türkkan, B. Sarıboğa, N. Sarıboğa, Synthesis, characterization and antimicrobial activity of 3,5-di-tertbutylsalicylaldehyde-S-methylthiosemicarbazones and their Ni(II) complexes, Transition. Met. Chem. 36 (2011) 679–684.
[2] D.M. Boghaei, S. Mohebi, Synthesis, characterization and study of vanadyl tetradentate Schiff base complexes as catalyst in aerobic selective oxidation of olefins, J. Mol. Catal. A: Chem. 179 (2002) 41–51.
[3] P.G. Cozzi, Metal-Salen Schiff base complexes in catalysis: Practical aspects, Chem. Soc. Rev. 33 (2004) 410–421.
[4] K.S. Munawar, S. Ali, M.N. Tahir, N. Khalid, Q. Abbas, I.Z. Qureshi, S. Hussain, M. Ashfaq, Synthesis, spectroscopic characterization, X-ray crystal structure, antimicrobial, DNA-binding, alkaline phosphatase and insulin-mimetic studies of oxidovanadium(IV) complexes of azomethine precursors, J. Coord. Chem. 73 (2020) 2275–2300.
[5] M.R. Maurya, M. Kumar, S.J.J. Titinchi, H.S. Abbo, S. Chand, Oxovanadium(IV) Schiff base complexes encapsulated in zeolite-Y as catalysts for the liquid-phase hydroxylation of phenol, Catal. Lett. 86 (2003) 97–105.
[6] T.A. Alsalim, J.S. Hadi, E.A. Al-Nasir, H.S. Abbo, S.J.J. Titinchi, Hydroxylation of phenol catalyzed by oxovanadium(IV) of Salen-type Schiff base complexes with hydrogen peroxide, Catal. Lett. 136 (2010) 228–233.
[7] A.P. de Azevedo Marques, E.R. Dockal, F.C. Skrobot, I.L. Viana Rosa, Synthesis, characterization and catalytic study of [N, N′-bis(3-ethoxysalicylidene)-m-xylylenediamine]oxovanadium(IV) complex, Inorg. Chem. Commun. 10 (2007) 255–261.
[8] S. Bunce, R.J. Cross, L.J. Farrugia, S. Kunchandy, L.L. Meason, K.W. Muir, M. O'Donnel, R.D. Peacock, D. Stirling, S.J. Teat, Chiral Schiff base complexes of copper(II), vanadium(IV) and nickel(II) as oxidation catalysts. X-ray crystal structures of [cu(R-salpn)(OH₂)] and [cu(±−busalcx)], Polyhedron 17 (1998) 4179–4187.
[9] K.S. Munawar, S. Ali, M.N. Tahir, N. Khalid, Q. Abbas, I. Qureshi, S. Shahzadi, Investigation of derivatized Schiff base ligands of 1,2,4-triazole amine and their oxovanadium(IV) complexes: Synthesis, structure, DNA binding, alkaline phosphatase inhibition, biological screening, and insulin mimetic properties, Russ. J. Gen. Chem. 85 (2015) 2183–2197.
[10] R.S. Walmsley, Z.R. Tshentu, Imidazole-based vanadium complexes as haloperoxidase models for oxidation reactions, S. Afr. J. Chem. 63 (2010) 95–104.
[11] S. Mohebbi, F. Nikpour, S. Raiati, Homogeneous green catalyst for epoxidation of cyclooctene by mono oxovanadium(IV) complexes of N₂O₂ donate ligand system, J. Mol. Catal. A: Chem. 256 (2006) 265–268.
[12] M.M. Cecchini, F. De Angelis, C. Iacobucci, S. Reale, M. Crucianelli, Ionic liquids vs conventional solvents: A comparative study in the selective catalytic oxidations promoted by oxovanadium(IV) complexes, Appl. Catal. A: Gen. 599 (2020), 117622.
[13] M. Mancka, W. Plass, Dioxomolybdenum(VI) complexes with amino acid functionalized N-salicylidene hydrazides: Synthesis, structure and catalytic activity, Inorg. Chem. Commun. 10 (2007) 677–680.
[14] M. Salavati-Niasari, M. Bazarganipour, Effect of single-wall carbon nanotubes on direct epoxidation of cyclohexene catalyzed by new derivatives of cis-dioxomolybdenum(VI) complexes with bis-bidentate Schiff-base containing aromatic nitrogen–nitrogen linkers, J. Mol. Catal. A: Chem. 278 (2007) 173–180.
[15] Y.D. Li, X.K. Fu, B.W. Gong, X.C. Zou, X.B. Tu, J.X. Chen, Synthesis of novel immobilized tridentate Schiff base dioxomolybdenum(VI) complexes as efficient and reusable catalysts for epoxidation of unfunctionalized olefins, J. Mol. Catal. A: Chem. 322 (2010) 55–62.
[16] Y. Yang, Y. Zhang, S.J. Hao, Q.B. Kan, Periodic mesoporous organosilicas with bis (8-quinolinolato) dioxomolybdenum(VI) inside the channel walls, J. Colloid Interface Sci. 362 (2011) 157–163.
[17] S.M. Bruno, J.A. Fernandes, L.S. Martins, I.S. Gonç̧alves, M. Pillinger, P. Ribeiro-Claro, J. Rocha, A.A. Valente, Dioxomolybdenum(VI) modified mesoporous materials for the catalytic epoxidation of olefins, Catal. Today 114 (2006) 263–271.
[18] C.Y. Lorber, S.P. Smidt, J.A. Osborn, Selective and environmentally benign aerobic catalytic oxidation of alcohols by a molybdenum-copper system, Eur. J. Inorg. Chem. 655–658 (2000).
[19] R.A. Sheldon, J.K. Kochi, Metal-catalyzed Oxidation of Organic Compounds, Academic Press, New York, 1981.
[20] M. Musawir, P.N. Davey, G. Kelly, I.V. Kozhevnikov, Highly efficient liquid-phase oxidation of primary alcohols to aldehydes with oxygen catalysed by Ru–Co oxide, Chem. Commun. 12 (2003) 1414–1415.
[21] M. Hudlicky, Oxidation in Organic Chemistry, ACS Monograph Series, ACS, Washington, 1990.
[22] F.M. Menger, C. Lee, Synthetically useful oxidations at solid sodium permanganate surfaces, Tetrahedron Lett. 22 (1981) 1655–1656.
[23] K.C. Lee, B.S. Koo, Y.S. Lee, H.K. Cho, K.J. Lee, Oxidation and bromodehydroxymethylation of benzylic alcohols using NaBr ₀3/NaHSO3 reagent, Bull. Korean Chem. Soc. 23 (2002) 1667–1670.
[24] A. Rostami, O. Pourshiani, N. Darvishi, B. Atashkar, Efficient and green oxidation of alcohols with tert-butyl hydrogenperoxide catalyzed by a recyclable magnetic

core-shell nanoparticle-supported oxo-vanadium ephedrine complex, C. R. Chim. 20 (2017) 435–439.

[25] M.B. Smith, March's advanced organic chemistry: reactions, mechanisms, and structure, John Wiley & Sons, 2020.

[26] N. Bhati, K. Sarma, A. Goswami, Expedient method for oxidation of alcohol by hydrogen peroxide in the presence of Amberlite IRA 400 resin (basic) as phase-transfer catalyst, Synth. Commun. 38 (2008) 1416–1424.

[27] J.J. Boruah, S.P. Das, Solventless, selective and catalytic oxidation of primary, secondary and benzylic alcohols by a Merrifield resin supported molybdenum(vi) complex with $H_2O_2$ as an oxidant, RSC Adv. 8 (2018) 34491–34504.

[28] V. Mahdavi, M. Mardani, Selective oxidation of benzyl alcohol with tert-butylhydroperoxide catalysed via Mn (II) 2,2-bipyridine complexes immobilized over the mesoporous hexagonal molecular sieves (HMS), J. Chem. Sci. 124 (2012) 1107–1115.

[29] C. Parmeggiani, F. Cardona, Transition metal based catalysts in the aerobic oxidation of alcohols, Green Chem. 14 (2012) 547–564.

[30] L.H. Abdel-Rahman, A.M. Abu-Dief, M.S.S. Adam, S.K. Hamdan, Some new nano-sized mononuclear Cu(II) Schiff base complexes: Design, characterization, molecular modeling and catalytic potentials in benzyl alcohol oxidation, Catal. Lett. 146 (2016) 1373–1396.

[31] A. Bordoloi, S. Sahoo, F. Lefebvre, S. Halligudi, Heteropoly acid-based supported ionic liquid-phase catalyst for the selective oxidation of alcohols, J. Catal. 259 (2008) 232–239.

[32] P. Maity, C.S. Gopinath, S. Bhaduri, G.K. Lahiri, Applications of a high performance platinum nanocatalyst for the oxidation of alcohols in water, Green Chem. 11 (2009) 554–561.

[33] S. Putla, M.H. Amin, B.M. Reddy, A. Nafady, K.A. Al Farhan, S.K. Bhargava, $MnO_x$ nanoparticle-dispersed $CeO_2$ nanocubes: A remarkable hetero nanostructured system with unusual structural characteristics and superior catalytic performance, ACS Appl. Mater. Interfaces 7 (2015) 16525–16535.

[34] R. Poreddy, C. Engelbrekt, A. Riisager, Copper oxide as efficient catalyst for oxidative dehydrogenation of alcohols with air, Catal. Sci. Technol. 5 (2015) 2467–2477.

[35] X.J. Meng, K.F. Lin, X.Y. Yang, Z.H. Sun, D.Z. Jiang, F.S. Xiao, Catalytic oxidation of olefins and alcohols by molecular oxygen under air pressure over $Cu_2(OH)PO_4$ and $Cu_4O(PO_4)_2$ catalysts, J. Catal. 218 (2003) 460–464.

[36] L.H. Abdel-Rahman, M.S.S. Adam, A.M. Abu-Dief, A.A.H. Abdel-Mawgoud, Catalytic potential of new mononuclear Cr(III)-Imine complexes for selective oxidation of benzyl alcohol by aqueous $H_2O_2$, J. Transit. Met. Complexes 2 (2019) 1–13.

[37] S. Das, T. Punniyamurthy, Cobalt(II)-catalyzed oxidation of alcohols into carboxylic acids and ketones with hydrogen peroxide, Tetrahedron Lett. 44 (2003) 6033–6035.

[38] J.E. Remias, A. Sen, Palladium-mediated aerobic oxidation of organic substrates: the role of metal versus hydrogen peroxide, J. Mol. Catal. A: Chem. 189 (2002) 33–38.

[39] Y. Shvo, V. Goldman-Lev, Catalytic oxidation of alcohols with allyl diethyl phosphate and palladium acetate, J. Organomet. Chem. 650 (2002) 151–156.

[40] J. Zhu, P.C. Wang, M. Lu, Selective oxidation of benzyl alcohol under solvent-free condition with gold nanoparticles encapsulated in metal-organic framework, Appl. Catal. A: Gen. 477 (2014) 125–131.

[41] G. Urgoitia, G. Galdón, F. Churruca, R. SanMartin, M.T. Herrero, E. Domínguez, Aerobic oxidation of secondary benzyl alcohols catalyzed by phosphinite-based palladium pincer complexes, Environ. Chem. Lett. 16 (2018) 1101–1108.

[42] Y. Xie, W.M. Mo, D. Xu, Z.L. Shen, N. Sun, B.X. Hu, X.Q. Hu, Efficient NO Equivalent for Activation of Molecular Oxygen and Its Applications in Transition-Metal-Free Catalytic Aerobic Alcohol Oxidation, J. Org. Chem. 72 (2007) 4288–4291.

[43] A. Allahresani, E. Naghdi, M.A. Nasseri, K. Hemmat, Selective oxidation of alcohols and sulfides via $O_2$ using a Co (II) salen complex catalyst immobilized on KCC-1: synthesis and kinetic study, RSC Adv. 10 (2020) 37974–37981.

[44] J.U. Ahmad, M.T. Raisanen, M. Leskela, T. Repo, Copper catalyzed oxidation of benzylic alcohols in water with $H_2O_2$, Appl. Catal. A: Gen. 411–412 (2012) 180–187.

[45] S. Verma, R. Singh, D. Tripathi, P. Gupta, G.M. Bahuguna, S.L. Jain, Thiourea dioxide with TBHP: a fruitful and greener recipe for the catalytic oxidation of alcohols, RSC Adv. 3 (2013) 4184–4188.

[46] C. Bhaumik, D. Steina, S. Vincendeau, R. Poli, E. Manoury, Oxidation of alcohols by TBHP in the presence of sub-stoichiometric amounts of $MnO_2$, C. R. Chim. 19 (2016) 566–570.

[47] M. Sutradhar, L.M.D.R.S. Martins, M.F.C.G. daSilva, A.J.L. Pombeiro, Oxidovanadium complexes with tridentate aroylhydrazone as catalyst precursors for solvent-free microwave-assisted oxidation of alcohols, Appl. Catal. A: Gen. 493 (2015) 50–57.

[48] B. Chen, X. Huang, B. Wang, Z. Lin, J. Hu, Y. Chi, C. Hu, Three new imidazole-functionalized hexanuclear oxidovanadium clusters with exceptional catalytic oxidation properties for alcohols, Chem. Eur. J. 19 (2013) 4408–4413.

[49] S. Verma, J.L. Bras, S.L. Jain, J. Muzart, Thiol-yne click on nano-starch: An expedient approach for grafting of oxo-vanadium Schiff base catalyst and its use in the oxidation of alcohols, Appl. Catal. A: Gen. 468 (2013) 334–340.

[50] S.R. Reddy, S. Das, T. Punniyamurthy, Polyaniline supported vanadium catalyzed aerobic oxidation of alcohols to aldehydes and ketones, Tetrahedron Lett. 45 (2004) 3561–3564.

[51] M. Dabiri, M. Koohshari, F. Shafipour, M. Kasmaei, P. Salari, D. MaGee, Supported vanadium Schiff bases complex on nano silica: a heterogeneous catalyst for the selective oxidation of sulfides and alcohols, J. Iran. Chem. Soc. 13 (2016) 1265–1272.

[52] B. Gao, M. Wan, J. Men, Y. Zhang, Aerobic selective oxidation of benzyl alcohols to benzaldehyde catalyzed by bidentate Schiff base dioxomolybdenum(VI) complex immobilized on CPS microspheres, Appl. Catal. A: Gen. 439 (2012) 156–162.

[53] S. Verma, M. Nandi, A. Modak, S.L. Jain, A. Bhaumik, Novel organic-inorganic hybrid mesoporous silica supported oxo-vanadium Schiff base for selective oxidation of alcohols, Adv. Synth. Catal. 353 (2011) 1897–1902.

[54] L. Rivoira, M.L. Martínez, O. Anunziata, A. Beltramone, Vanadium oxide supported on mesoporous SBA-15 modified with Al and Ga as a highly active catalyst in the ODS of DBT, Micropor. Mesopor. Mater. 254 (2017) 96–113.

[55] C.J. Carrasco, F. Montilla, E. Álvarez, C. Mealli, G. Manca, A. Galindo, Experimental and theoretical insights into the oxodiperoxomolybdenum-catalysed sulphide oxidation using hydrogen peroxide in ionic liquids, Dalton Trans. 43 (2014) 13711–13730.

[56] L. Balapoor, R. Bikas, M. Dargahi, Catalytic oxidation of benzyl-alcohol with $H_2O_2$ in the presence of a dioxidomolybdenum (VI) complex, Inorg. Chim. Acta 510 (2020), 119734.

[57] H. Kargar, Synthesis, characterization and crystal structure of a manganese(III) Schiff base complex and investigation of its catalytic activity in the oxidation of benzylic alcohols, Transition Met. Chem. 39 (2014) 811–817.

[58] M. Hatefi, M. Moghadam, I. Sheikhshoaei, V. Mirkhani, S. Tangestaninejad, I. Mohammadpoor-Baltork, H. Kargar, Ru(salophen)Cl supported on polystyrene-bound imidazole: An efficient and robust heterogeneous catalyst for epoxidation of alkenes with sodium periodate, Appl. Catal. A: Gen. 370 (2009) 66–71.

[59] M. Moghadam, V. Mirkhani, S. Tangestaninejad, I. Mohammadpoor-Baltork, H. Kargar, I. Sheikhshoaei, Highly efficient epoxidation of alkenes with sodium periodate catalyzed by reusable polystyrene-bound Ruthenium(III) salophen, J. Iran. Chem. Soc. 8 (2011) 1019–1029.

[60] H. Kargar, Rapid and efficient biomimetic oxidation of 2-imidazolines to their corresponding imidazoles with $NaIO_4$ catalyzed by Mn(salophen)Cl, Inorg. Chem. Commun. 14 (2011) 863–866.

[61] X-AREA, version 1.30, program for the acquisition and analysis of data, Stoe & Cie GmbH, Darmstadt, Germany, (2005).

[62] X-RED, version 1.28b, program for data reduction and absorption correction, Stoe & Cie GmbH, Darmstadt, Germany, (2005).

[63] X-SHAPE, version 2.05, program for crystal optimization for numerical absorption correction, Stoe & Cie GmbH, Darmstadt, Germany, (2004).

[64] R.H. Blessing, An empirical correction for absorption anisotropy, Acta Crystallogr, A 51 (1995) 33–38.

[65] M.C. Burla, R. Caliandro, M. Camalli, B. Carrozzini, G.L. Cascarano, L. De Caro, C. Giacovazzo, G. Polidori, R. Spagna, SIR2004: an improved tool for crystal structure determination and refinement, J. Appl. Crystallogr. 38 (2005) 381–388.

[66] G.M. Sheldrick, A short history of SHELX, Acta Crystallogr. A 64 (2008) 112–122.

[67] M.J. Frisch, G.W. Trucks, H.B. Schlegel, G.E. Scuseria, M.A. Robb, J.R. Cheeseman, G. Scalmani, V. Barone, B. Mennucci, G.A. Petersson, H. Nakatsuji, M. Caricato, X. Li, H.P. Hratchian, A.F. Izmaylov, J. Bloino, G. Zheng, J.L. Sonnenberg, M. Hada, M. Ehara, K. Toyota, R. Fukuda, J. Hasegawa, M. Ishida, T. Nakajima, Y. Honda, O. Kitao, H. Nakai, T. Vreven, J.A. Montgomery, Jr., J.E. Peralta, F. Ogliaro, M. Bearpark, J.J. Heyd, E. Brothers, K.N. Kudin, V.N. Staroverov, T. Keith, R. Kobayashi, J. Normand, K. Raghavachari, A. Rendell, J.C. Burant, S.S. Iyengar, J. Tomasi, M. Cossi, N. Rega, J.M. Millam, M. Klene, J.E. Knox, J.B. Cross, V. Bakken, C. Adamo, J. Jaramillo, R. Gomperts, R.E. Stratmann, O. Yazyev, A.J. Austin, R. Cammi, C. Pomelli, J.W. Ochterski, R.L. Martin, K. Morokuma, V.G. Zakrzewski, G. A. Voth, P. Salvador, J.J. Dannenberg, S. Dapprich, A.D. Daniels, O. Farkas, J.B. Foresman, J.V. Ortiz, J. Cioslowski, D.J. Fox, GAUSSIAN 09 (Revision D.01), Gaussian, Inc., Wallingford, CT (2013).

[68] A.D. Becke, Density-functional thermochemistry. III. The role of exact exchange, J. Chem. Phys. 98 (1993) 5648–5652.

[69] J. Tomasi, B. Mennucci, R. Cammi, Quantum mechanical continuum solvation models, Chem. Rev. 105 (2005) 2999–3093.

[70] F. Weigend, R. Ahlrichs, Balanced basis sets of split valence, triple zeta valence and quadruple zeta valence quality for H to Rn: Design and assessment of accuracy, Phys. Chem. Chem. Phys. 7 (2005) 3297–3305.

[71] J. Gauss, Effects of electron correlation in the calculation of nuclear magnetic resonance chemical shifts, J. Chem. Phys. 99 (1993) 3629–3643.

[72] http://www.chemissian.com.

[73] M.R. Maurya, S. Agarwal, C. Bader, M. Ebel, D. Rehder, Synthesis, characterisation and catalytic potential of hydrazonato-vanadium(V) model complexes with $[VO]^{3+}$ and $[VO_2]^+$ cores, Dalton Trans. 537–544 (2005).

[74] S.D. Kurbah, M. Asthana, I. Syiemlieh, A.A. Lywait, M. Longchar, R.A. Lal, New dioxido-vanadium(V) complexes containing hydrazone ligands: Syntheses, crystal structure and their catalytic application toward C-H bond functionalization, J. Organomet. Chem. 876 (2018) 10–16.

[75] Y. Li, L. Xu, M. Duan, J. Wu, Y. Wang, K. Dong, M. Han, Z. You, An acetohydroxamate-coordinated oxidovanadium(V) complex derived from pyridinohydrazone ligand with urease inhibitory activity, Inorg. Chem. Commun. 105 (2019) 212–216.

[76] S. Gao, X.-F. Zhang, L.-H. Huo, H. Zhao, (Methanol-κO)[3-methoxysalicylaldehyde (4-methoxybenzoyl)hydrazonato(2–)-κ³O, O′, N]dioxomolybdenum(VI), Acta Crystallogr, E 60 (2004) m1731–m1733.

[77] A. Rana, R. Dinda, P. Sengupta, S. Ghosh, L.R. Falvello, Synthesis, characterisation and crystal structure of cis-dioxomolybdenum(VI) complexes of some potentially pentadentate but functionally tridentate (ONS) donor ligands, Polyhedron 21 (2002) 1023–1030.

[78] V. Vrdoljak, M. Cindric, D. Milic, D. Matkovic-Calogovic, P. Novak, B. Kamenar, Synthesis of five new molybdenum(VI) thiosemicarbazonato complexes. Crystal structures of salicylaldehyde and 3-methoxy-salicylaldehyde 4-methylthiosemicarbazones and their molybdenum(VI) complexes, Polyhedron 24 (2005) 1717–1726.

[79] M.A. Wolff, S.K. Grimwood, D.J. McKinnon, J.J. Turner, M.J. Jayatilaka, D. Spackman, Crystal Explorer 17.5, University of Western Australia, 2012.

[80] M.A. Spackman, D. Jayatilaka, Hirshfeld surface analysis, CrystEngComm. 11 (2009) 19–32.

[81] M.N. Tahir, M. Ashfaq, F. Alexander, J. Caballero, E.W. Hernández-Rodríguez, A. Ali, Rationalizing the stability and interactions of 2, 4-diamino-5-(4-chloro-phenyl)-6-ethylpyrimidin-1-ium 2-hydroxy-3, 5-dinitrobenzoate salt, J. Mol. Struct. 1193 (2019) 185–194.

[82] A. Ali, M. Khalid, M. Fayyaz ur Rehman, S. Haq, A. Ali, M.N. Tahir, M. Ashfaq, F. Rasool, A.A.C. Braga, Efficient synthesis, SC-XRD, and theoretical studies of o-benzenesulfonylated pyrimidines: Role of noncovalent interaction influence in their supramolecular network, ACS omega 25 (2020) 15115–15128.

[83] M. Khalid, A. Ali, J. Tariq, M.N. Tahir, H. Asghar, R. Aliabad, I. Hussain, M. Ashfaq, M.U. Khan, Stabilization of supramolecular assembly of N-substituted benzylidene acetohydrazide analogs by non-covalent interactions: A concise experimental and theoretical approach, ChemistrySelect 5 (2020) 10618–10631.

[84] M. Murtaza, M.N. Ahmed, M. Hafeez, M. Ashfaq, M.N. Tahir, D.M. Gil, B. Galmes, S. Hameed, A. Frontera, Recurrent π–π stacking motifs in three new 4, 5-dihydro-pyrazolyl-thiazole-coumarin hybrids: X-ray characterization, Hirshfeld surface analysis and DFT calculations, New J. Chem. 44 (2020) 14592–14603.

[85] J.J. McKinnon, D. Jayatilaka, M.A. Spackman, Towards quantitative analysis of intermolecular interactions with Hirshfeld surfaces, Chem. Commun. 3814–3816 (2007).

[86] A. Ali, M. Khalid, S. Abid, M.N. Tahir, J. Iqbal, M. Ashfaq, F. Kanwal, C. Lu, Green synthesis, SC-XRD, non-covalent interactive potential and electronic communication via DFT exploration of pyridine-based hydrazone, Crystals 10 (2020) 778–797.

[87] M. Khalid, A. Ali, S. Haq, M.N. Tahir, J. Iqbal, A.A.C. Braga, M. Ashfaq, S. U. Akhtar, O-4-Acetylamino-benzenesulfonylated pyrimidine derivatives: synthesis, SC-XRD, DFT analysis and electronic behaviour investigation, J. Mol. Struct. 1224 (2020), 129308.

[88] M. Khalid, A. Ali, S. Abid, M.N. Tahir, M.U. Khan, M. Ashfaq, Facile ultrasound-based synthesis, SC-XRD, DFT exploration of the substituted acyl-hydrazones: An experimental and theoretical slant towards supramolecular, Chemistryselect 5 (2020) 14844–14856.

[89] M. Ashfaq, G. Bogdanov, V. Glebov, A. Ali, M.N. Tahir, S. Abdullah, Single crystal investigation, Hirshfeld surface analysis and DFT exploration of the pyrimethamine-based novel organic salt: 2,4-diamino-5-(4-chlorophenyl)-6-ethyl-pyrimidin-1-ium, 3-carboxybenzoate hydrate (1:1:1), J. Mol. Struct. 1224 (2021), 129309.

[90] V. Vrdoljak, B. Prugovecki, D.M. Calogovic, J. Pisk, R. Dreos, P. Siega, Supramolecular hexagon and chain coordination polymer containing the $MoO_2^{2+}$ core: Structural transformation in the solid state, Cryst. Growth Des. 11 (2011) 1244–1252.

[91] R. Kia, H. Kargar, Synthesis, spectral characterization and crystal structure studies of a new hydrazone Schiff base and its dioxomolybdenum(VI) complex, J. Coord. Chem. 68 (2015) 1441–1451.

[92] G. Romanowski, T. Lis, Chiral oxidovanadium(V) complexes with tridentate Schiff bases derived from S(+)-2-amino-1-propanol: Synthesis, structure, characterization and catalytic activity, Inorg. Chim. Acta 394 (2013) 627–634.

[93] C. Cordelle, D. Agustin, J.C. Daran, R. Poli, Oxo-bridged bis oxo-vanadium(V) complexes with tridentate Schiff base ligands $(VOL)_2O$ (L = SAE, SAMP, SAP): Synthesis, structure and epoxidation catalysis under solvent-free conditions, Inorg. Chim. Acta 364 (2010) 144–149.

[94] J. Hartung, S. Drees, M. Grab, P. Schmidt, I. Svoboda, H. Fuess, A. Murso, D. Stalke, (Schiff-base)vanadium(V) complex-catalyzed oxidations of substituted bis (homoallylic) alcohols–stereoselective synthesis of functionalized tetrahydrofurans, Eur. J. Org. Chem. (2003) 2388–2408.

[95] M. Bagherzadeh, M. Amini, H. Parastar, M. Jalali-Heravi, A. Ellern, L.K. Woo, Synthesis, X-ray structure and oxidation catalysis of a oxido–peroxido molybdenum(VI) complex with a tridentate Schiff base ligand, Inorg. Chem. Commun. 20 (2012) 86–89.

[96] M.A. Palafox, DFT computations on vibrational spectra: Scaling procedures to improve the wavenumbers, Phys. Sci. Rev. 3 (2018) 1–30.

[97] T.M. Asha, M.R.P. Kurup, Synthesis, spectral characterization and crystal structures of dioxidomolybdenum(VI) complexes derived from nicotinoylhydrazones, J. Chem. Crystallogr. 49 (2019) 219–231.

[98] N. Noshiranzadeh, M. Mayeli, R. Bikas, K. Ślepokura, T. Lis, Selective catalytic oxidation of benzyl alcohol to benzaldehyde by a mononuclear oxovanadium(V) complex of a bis(phenolate)ligand containing bulky tert-butyl substituents, Transition Met. Chem. 39 (2014) 33–39.

[99] M. Hatefi-Ardakani, S. Saeednia, Z. Pakdin-Parizi, M. Rafeezadeh, Efficient and selective oxidation of alcohols with tert-BuOOH catalyzed by a dioxomolybdenum (VI) Schiff base complex under organic solvent-free conditions, Res. Chem. Intermed. 42 (2016) 7223–7230.